Low methane concentrations in sediment along the continental slope north of Siberia: Inference from pore water geochemistry

Clint M. Miller[1], Gerald R. Dickens[1], Martin Jakobsson[2], Carina Johansson[2], Andrey Koshurnikov[3], Matt O'Regan[2], Francesco Muschitiello[4], Christian Stranne[2], Carl-Magnus Mörth[2]

A revised manuscript submitted to:

Biogeosciences

[February 20, 2017]

[1]Department of Earth Science, Rice University, Houston, TX, USA

[2]Department of Geological Sciences, Stockholm University, Stockholm, Sweden

[3]V.I. Il'ichev Pacific Oceanological Institute, RAS

[4]Lamont-Doherty Earth Observatory, Columbia University, NY, USA

Correspondence to: Clint M. Miller (clint.m.miller@rice.edu)

Abstract: The Eastern Siberian Margin (ESM), a vast region of the Arctic, potentially holds large amounts of methane (CH_4) in sediments as gas hydrate and free gas. Although this methane has become a topic of discussion, the ESM remains sparingly explored. Here we present pore water chemistry results from 32 cores taken during Leg 2 of the 2014 SWERUS-C3 expedition. The cores come from depth transects across the slope and rise sediments off the Chukchi and East Siberian Sea (CESS) of the ESM between Wrangel Island and the New Siberian Islands. Upward CH_4 flux towards the seafloor, as inferred from profiles of dissolved sulfate (SO_4^{2-}), alkalinity, and the $\delta^{13}C$ of dissolved inorganic carbon (DIC), is negligible at all stations east of where the Lomonosov Ridge abuts the ESM at about 143°E longitude. In the upper eight meters of these cores, downward sulfate flux never exceeds 6.2 mol/m^2-kyr, the upward alkalinity flux never exceeds 6.8 mol/m^2-kyr, and $\delta^{13}C$-DIC only slowly decreases with depth (-3.6‰/m on average). Moreover, upon addition of Zn acetate to pore water samples, ZnS did not precipitate, indicating a lack of dissolved H_2S. Phosphate, ammonium, and metal profiles reveal that metal oxide reduction by organic carbon dominates the geochemical environment, and supports very low organic carbon turnover rates. A single core on Lomonosov Ridge differs, as diffusive fluxes for SO_4^{2-} and alkalinity were 13.9 and 11.3 mol/m^2-kyr, respectively, the $\delta^{13}C$-DIC gradient was 5.6‰/m, and Mn^{2+} reduction terminated within 1.3 m of the seafloor. These are among the first pore water results generated from this vast climatically sensitive region, and they imply that abundant CH_4, including gas hydrates, do not characterize the CESS continental slope. This contradicts previous modeling and discussion, which generally have assumed the widespread presence of CH_4.

1. Introduction

The Arctic is especially sensitive to global climate change, and over the last century has experienced anomalous warming (Serreze et al., 2000; Peterson et al., 2002; Semiletov et al., 2004). Past and future increases in atmospheric and surface water temperatures should, with time, lead to significant warming of intermediate to deep waters (Dmitrenko et al., 2008; Spielhagen et al., 2011), as well as sediment beneath the seafloor (Reagan and Moridis, 2009; Phrampus et al., 2014). The latter is both fascinating and worrisome, because pore space within the upper few hundreds of meters of sediment along many continental slopes can contain large amounts of temperature-sensitive methane (CH_4) in the form of gas hydrates, free gas, and dissolved gas (Kvenvolden, 1993 and 2001; Beaudoin et al., 2014). Consequently, numerous papers have discussed the potential impact of future warming upon CH_4 within slope sequences of the Arctic Ocean (Paull et al., 1991; Archer, 2007; Reagan and Moridis, 2008; McGuire et al., 2009; Biastoch et al., 2011; Elliott et al., 2011; Ferré et al., 2012; Giustiniani et al., 2013; Thatcher et al., 2013; Stranne et al., 2016).

Globally, the amount and distribution of CH_4 in sediment along continental slopes remains poorly constrained (Beaudoin et al., 2014). This is particularly true for the Arctic Ocean, because ice cover makes accessibility to many regions difficult. Nonetheless, numerous papers have inferred enormous quantities of gas hydrate surrounding the Arctic (Kvenvolden and Grantz, 1990; Max and Lowrie, 1993; Buffett and Archer, 2004; Klauda and Sandler, 2005; Max and Johnson, 2012; Wallmann et al., 2012; Piñero et al., 2013; Fig. 1 and 2). In some sectors, compelling evidence exists for abundant sedimentary CH_4 and gas hydrate. Bottom simulating reflectors (BSRs) on seismic profiles generally mark the transition between overlying gas hydrate and underlying free gas (Holbrook et al., 1996; Pecher et al., 2001), and thereby imply

high quantities of CH_4 in pore space (Dickens et al., 1997; Pecher et al., 2001). Such BSRs have been documented along the North Slope of Alaska (Collett, 2002; Collett et al., 2010), within the Beaufort Sea (Grantz et al., 1976; Grantz et al., 1982; Weaver and Stewart, 1982; Hart et al., 2011; Phrampus et al., 2014), around Canadian Arctic Islands (Judge, 1982; Hyndman and Dallimore, 2001; Majorowicz and Osadetz, 2001; Yamamoto and Dallimore, 2008), adjacent to Svalbard (Eiken and Hinz, 1993; Posewang and Mienert, 1999; Vanneste et al., 2005; Hustoft et al., 2009; Petersen et al., 2010), and within the Barents Sea (Andreassen et al. 1990; Løvø et al., 1990; Laberg and Andreassen, 1996; Laberg et al., 1998; Chand et al., 2008; Ostanin et al., 2013). Furthermore, Lorenson and Kvenvolden (1995) observed high CH_4 concentrations in shelf waters of the Beaufort Sea, and Shakhova (2010a, 2010b) have documented CH_4 escape to the water column above the East Siberian shelf. It generally has been assumed that sediment on the ESM slope contains copious CH_4 and gas hydrate (Fig. 1), although there is little data to support or refute this idea.

Regional assessments for the presence of abundant CH_4 in marine sediment can be acquired through two general approaches. The first includes geophysical applications, primarily seismic reflection profiling and the recognition of BSRs (MacKay et al., 1994; Carcione and Tinivella, 2000; Haacke et al., 2008), which are a common, but not ubiquitous feature, of hydrate bearing sediments. The second utilizes chemical analyses of pore waters obtained from sediment cores (Borowski et el., 1996; Borowski et al., 1999; Kastner et al., 2008b; Dickens and Snyder 2009). In marine sediments with abundant CH_4, a general and important process occurs near the seafloor; typically, within the upper 30 m. Microbes utilize upward migrating CH_4 and downward diffusing sulfate (SO_4^{2-}) via anaerobic oxidation of methane (AOM; e.g., Barnes and Goldberg, 1976; Reeburgh, 1976; Devol and Ahmed, 1981; Boetius et al., 2000):

$$CH_4 + SO_4^{2-} \rightarrow HS^- + HCO_3^- + H_2O \quad (1)$$

The reaction leads to characteristic pore water chemistry profiles, ones with a clearly recognizable sulfate-methane transition (SMT; Fig. 3). The depth of the SMT inversely relates to the flux of CH_4, which in turns relates to the distribution of CH_4 beneath the seafloor (Borowski et al., 1999; Dickens, 2001; Bhatnagar, 2011). Where CH_4 fluxes toward the seafloor are high, the SMT is located at shallow depth. For example, along the continental shelf and slope of the Beaufort Sea, where seismic profiles indicate gas hydrate. Coffin et al. (2008, 2013) predictably have documented SMTs in shallow sediment (< 10 mbsf).

The joint Swedish, Russian, U.S. Arctic Ocean Investigation of Climate-Cryosphere-Carbon interaction (SWERUS-C3) project is aimed at understanding spatial changes in carbon cycling across the ESM. A central theme concerns the amount, distribution, and fluxes of CH_4, and the overall project included two expedition legs in the boreal summer of 2014 using the Swedish icebreaker *IB Oden*. Between August 21 and October 5, Leg 2 sailed between Barrow, Alaska and Tromsø, Norway, focusing on the continental slope of the ESM. SWERUS Leg 2 included geophysical surveying and retrieval of numerous sediment cores, of which 446 pore water samples from eight piston, seven gravity, and 17 multicores (Fig. 2) are studied here to ascertain potential fluxes of CH_4 toward the seafloor

2. Background

2.1 East Siberian margin geology

Extensive continental shelves and their associated slopes nearly encircle the Arctic Ocean (**Figure 1**). Although it represents only 2.6% of the world's ocean by area (Jakobsson, 2002), the present Arctic Ocean receives approximately 10% of the global freshwater input (Stein, 2008) as

well as corresponding massive discharge of terrigenous material (>249 Mt/yr; Holmes et al., 2002). Only Fram Strait allows deep-water flow to and from the Arctic Ocean. This strait, located between Greenland and Svalbard (Fig. 1), has a modern sill depth of about 2540 m (Jakobsson et al., 2003). It opened during the early to middle Miocene (Jakobsson et al., 2007; Engen et al., 2008; Hustoft et al., 2009). Prior to this, the Arctic Ocean only was connected to other oceans through shallow seaways (e.g., Turgay Straight), such that deep waters may have been anoxic for long intervals of the Cretaceous and Paleogene (Clark, 1988; O'Regan et al., 2011).

The ESM is defined here to comprise the margin of the East Siberian Sea, which stretches between Wrangel Island to the east and the New Siberian Islands to the west (Fig. 2). We include the adjacent Chukchi and East Siberian Sea (CESS) continental slope in the ESM. This continental shelf within this region is the widest in the world, extending 1500 km north from the coast. The enormous swath laying in water depths less than 100 m (~987 x 10^3 km^2; Jakobsson, 2002) was likely covered in km-thick ice shelf during marine isotope stage 6 (~140 ka), contributing to extensive formation of submarine permafrost (Judge, 1982; Weaver and Stewart, 1982; Løvø et al., 1990; Collett et al., 2010; Jakobsson et al., 2016). The expansive shelf contrasts with the relatively narrow continental slope, which intersects two ridge systems, Mendeleev Ridge to the east and Lomonosov Ridge to the west (Jakobsson et al., 2008). Bounded by these two ridge systems, the steep ESM slope leads into the gently sloping Chukchi, Arlis, and Wrangel perched continental rises (Jakobsson et al., 2003).

2.2 Regional oceanography

Bottom waters impinging the slope of the ESM generally can be divided into three masses: the Pacific Halocline (~50-200m), the Atlantic Layer (~200-800m), and Canada Basin Bottom Water (>800m; Timokhov, 1994; Rudels et al., 2000). The Pacific Halocline is a cold (-1.5-0°C), low salinity (32-33.5 psu) water mass that serves as a boundary (and heat sink) between sea ice (above) and Atlantic Layer water (below; Aagaard, 1981; Aagaard and Carmack, 1989). The underlying Atlantic Layer is warmer (>0°C) but more saline (33.5-34.5 psu; Rudels et al., 2000). The Atlantic Layer originates from water arriving partly through Fram Strait and partly through St. Anna Trough. Canada Basin Bottom Water is colder (~-0.5°C) and relatively saline (~34.9 psu), with a residence time exceeding 300 years (Stein, 2008). Importantly, inflow from the Atlantic varies over time, which further influences the temperature of the Atlantic Layer along slopes of the central Arctic Ocean (Dmitrenko et al., 2009; Woodgate et al., 2001).

2.3 Current speculation on gas hydrates in the Arctic

Even during summer months over the last decade, 2-3 m of sea ice covers much of the Arctic Ocean adjacent to Siberia (Stroeve et al., 2012). This necessitates the use of large ice breaking vessels to explore the region. Consequently, limited geologic information exists regarding CESS continental slopes of the ESM. Four icebreaker expeditions, the 1995 Polarstern Expedition ARK-XI/1 (Rachor, 1995), the 1996 Arctic Ocean Expedition ARK-XII/1 (Augstein et al., 1997), the 2008 Polarstern Expedition ARK-XXIII/3 (Jokat, 2010), and the 2009 Russian-American RUSALCA Expedition (Bakhmutov et al., 2009) have retrieved geophysical data and sediment on or adjacent to the ESM slope.

So far, no drilling has occurred on CESS slope. However, the 2004 Arctic Coring Expedition (Backman et al., 2009) drilled and cored the central Lomonosov Ridge (Fig. 1). There

155 are also land based studies (Gualtier et al., 2005; Sher et al., 2005; Andreev et al., 2009), and
156 some public oil and gas exploration material, which provides indirect data on the shelf (Hovland
157 and Svensen, 2006).

158 Despite the paucity of ground-truth data, many researchers have predicted widespread and
159 abundant CH_4 along the CESS continental slope, as clearly shown by maps of conjectured gas
160 hydrate distribution in the Arctic (Fig. 1). This inference has arisen for two main reasons. First,
161 the integrated input of particulate organic carbon (POC) over time provides the ultimate source
162 of CH_4 in marine sediments (Kvenvolden and Grantz, 1990). Arctic slopes may contain high
163 POC contents, which accumulated prior to the opening of the Fram Strait (Jokat and Ickrath,
164 2015), or along with terrigenous material during interglacial intervals of the Quaternary
165 (Danyushevskaya et al., 1980; Clark, 1988; Darby, 1989; Moran et al., 2006; Archer, 2015).
166 Certainly, organic rich Eocene sediments have been documented on other Arctic margins and in
167 the ACEX cores on Lomonosov Ridge (Moran et al., 2006; Backman and Moran, 2009; O'Regan
168 et al., 2011, Alekseev, 1997; Naidu et al., 2000; Niessen et al., 2013). Second, the thickness of
169 the gas hydrate stability zone (GHSZ) depends on bottom water temperature and the geothermal
170 gradient (Dickens, 2001). Because of very low bottom water temperatures along the slope and
171 low regional geothermal gradients (O'Regan et al., 2016); an extensive volume of sediment can
172 host gas hydrate (Miles, 1995; Makogon, 2010).

173

174 *2.4 Pore water chemistry above methane-charged sediment sequences*

175 Pore water chemistry profiles provide a powerful means to constrain CH_4 abundance and
176 fluxes in marine sediment sequences (Borowski et al., 1996; Berg et al., 1998; Jørgensen et al.,
177 2001; Torres and Kastner, 2009; Treude et al., 2014). Such profiles are generated by extracting

178 interstitial water samples from sediment cores, and then measuring concentrations of dissolved
179 species.

180 In regions without significant advection of water, pore water profiles of various analytes
181 relate to Fick's law of diffusion and chemical reactions (e.g., Berner, 1977; Froelich et al., 1979;
182 Klump and Martens 1981; Boudreau, 1997; and Iverson and Jorgensen, 1993). The flux (*J*) of a
183 dissolved species through porous marine sediment can be calculated from the concentration
184 gradient by (Li & Gregory, 1974; Berner, 1975; Lerman, 1977):

185 $$J = -\varphi D_s \frac{\partial C}{\partial Z}, \quad (2)$$

186 where φ is porosity, D_s is the diffusivity of an ion in sediment at a specified temperature, C is
187 concentration, and Z is depth. Note that, as generally written, J is positive for upward fluxes and
188 negative for downward fluxes relative to the seafloor. In many locations, φ and D_s change only
189 moderately (<20%) in the upper tens of meters below the seafloor. However, abundant CH_4 in
190 sediment necessarily leads to a large concentration gradient toward the seafloor and a major
191 upward flux of CH_4. The consequent reaction with SO_4^{2-} via AOM (Eqn. 1) thus leads to a series
192 of flux changes in dissolved components (addition or removal), and predictable variations in
193 corresponding concentration profiles across a SMT (Alperin, 1988; Borowski et al., 1996;
194 Niewohner et al., 1998; Ussler and Paull, 2008; Dickens and Snyder, 2009; Chatterjee et al.,
195 2011; Regnier et al., 2011). In such regions, the depth of the SMT directly relates to the flux of
196 CH_4 from below (Jørgensen et al., 1990; Dickens, 2001; D'Hondt et al., 2002; Hensen et al.,
197 2003), largely because SO_4^{2-} concentrations at the seafloor are nearly constant throughout the
198 oceans.

199 Alternatively, at seafloor locations with significant upward advection of fluids, such as
200 above faults, pore water profiles become more complicated to model (Torres et al., 2002). This is

because multiphase fluid flow (free gas and liquid) rarely reaches steady-state. Additionally, both steady and pulsed multiphase flow physically alters sediments creating soupy or mousse-like textures and sometimes gas pockets. However, if the upward advecting fluids contain significant CH_4 (and no SO_4^{2-}), the SMT shoals toward the seafloor with respect to predictions from considerations of CH_4 diffusion alone (Dickens, 2001). This can be observed generally from the very shallow SMTs observed at locations of CH_4 seepage worldwide (e.g., Aharon and Fu, 2000).

Typically, in all regions and at many locations, the SMT is a thin (<3 m) depth horizon with major inflections in both CH_4 and SO_4^{2-} profiles (Fig. 3). Sulfate concentrations decrease from seawater values at the seafloor to zero at the SMT; by contrast, CH_4 concentrations rise from zero at the SMT to elevated values at depth.

Importantly, though, as one can infer from Equations 1 and 2, AOM affects additional species dissolved in pore water (Alperin et al., 1988; Jørgensen et al., 1990; Dickens, 2001; Hensen et al., 2003; Snyder et al., 2007). Dissolved HS^- and HCO_3^- concentrations necessarily increase across the SMT, so an inflection occurs in their concentration profiles. These two species contribute to total alkalinity of marine waters (Gieskes and Rogers, 1973; Haraldsson et al., 1997), which can be defined as:

$$Alk_T = [HCO_3^-] + 2[CO_3^{2-}] + [HS^-] + [B(OH)_4^-] + [OH^-] + [HPO_4^{2-}] + [NH_3] + [X]\,, \quad (3)$$

where X refers to several minor species. However, in shallow sediments found above almost all CH_4 charged systems, this can be expressed as:

$$Alk_T \approx [HCO_3^-] + [HS^-]\,, \quad (4)$$

223 Thus, with the production of HS^- and HCO_3^-, an inflection in Alk_T occurs across the SMT (Luff
224 and Wallmann 2003; Dickens and Snyder, 2009; Jørgensen and Parkes, 2010; Chatterjee et al.,
225 2011; Smith and Coffin, 2014; Ye et al., 2016).
226 Marked changes in pore water profiles of other components also typically occur across the
227 SMT (Fig. 3). Because CH_4 is greatly depleted in ^{13}C, due to isotope fractionation during
228 methanogenesis at depth (Whiticar, 1999; Paull et al., 2000), the conversion of CH_4 to HCO_3^-
229 (Eqn. 1) decreases the $\delta^{13}C$ of DIC across the SMT (Torres et al., 2007; Holler et al., 2009;
230 Chatterjee et al., 2011; Yoshinaga et al., 2014). However, the magnitude of this change in $\delta^{13}C$-
231 DIC is complicated because excess ^{13}C-enriched HCO_3^- (formed during methanogenesis and
232 subsequent reactions) can also rise from below (Snyder et al., 2007; Chatterjee et al., 2011).
233 Dissolved Ba^{2+} concentrations generally increase significantly just above the SMT. This is
234 because solid barite ($BaSO_4$), a ubiquitous component of marine sediment on continental slopes
235 (Dehairs et al., 1980; Dymond et al., 1992; Gingele and Dahmke, 1994), dissolves in the SO_4^{2-}-
236 depleted pore water and dissolved Ba^{2+} then diffuses back across the SMT (Dickens, 2001;
237 Riedinger et al., 2006; Nöthen and Kasten, 2011). Dissolved Ca^{2+} concentrations usually
238 decrease across the SMT. This is due to authigenic carbonate precipitation resulting from the
239 production excess HCO_3^- (Greinert et al., 2001; Luff and Wallmann 2003; Snyder et al., 2007).
240 Importantly, though, dissolved NH_4^+ concentrations exhibit no inflection across the SMT. This is
241 because while decomposition of particulate organic matter generates NH_4^+, AOM does not
242 (Borowski et al., 1996).
243 Studies at numerous locations demonstrate that characteristic pore water profiles delineate
244 sediment sequences with significant CH_4, including gas hydrate, in the upper few hundred meters
245 below the seafloor (Fig. 3). Good examples include: Baltic Sea (Jørgensen et al, 1990), Black

246 Sea (Jørgensen et al, 2004), Blake Ridge (Paull et al., 2000; Borowski et al., 2001), Cariaco
247 Trench (Reeburgh, 1976), Cascadia Margin (Torres and Kastner, 2009), Gulf of Mexico (Kastner
248 et al., 2008a; Hu et al., 2010; Smith and Coffin, 2014), Hydrate Ridge (Claypool et al., 2006),
249 offshore Namibia (Niewohner et al., 1998), offshore Peru (Donohue et al., 2006), South China
250 Sea (Luo et al., 2013; Hu et al., 2015), and Sea of Japan (Expedition Scientists, 2014). Moreover,
251 in regions dominated by diffusion, fluxes of dissolved CH_4 can be estimated through use of
252 Equation 2 from concentration profiles of multiple constituents (e.g., SO_4^{2-}, HCO_3^-, Ca^{2+}) and
253 knowledge of porosity and sedimentary diffusion constants (e.g., Niewohner et al., 1998; Snyder
254 et al., 2007). At sites with abundant CH_4 in the upper few hundred meters below the seafloor,
255 notably including sites with gas hydrate and sites in the Beaufort Sea, estimated values for $J$$CH_4$
256 and -$J$$SO_4^{2-}$ are universally high (> ~50 mol/m^2-kyr).
257
258 **3. Materials and Methods**
259 *3.1 SWERUS-C3 Expedition, Leg 2*
260 Leg 2 of SWERUS-C3 included four transects across the CESS continental slope (Fig. 2).
261 These transects were along Arlis Spur (TR-1), north of central East Siberia (TR-2), from close to
262 Henrietta Island to the Makarov Basin (TR-3), and on the Amerasian side of Lomonosov Ridge
263 (TR-4). Along each transect, scientific operations involved bathymetric mapping as well as
264 sediment coring at a series of stations. An additional coring station was located on Lomonosov
265 Ridge, near where this bathymetric high intersects the ESM.
266 An array of coring techniques were used along each transect. In total, 50 sediment cores
267 were collected at 34 coring stations. These included: multicore sets (22), gravity cores (23),
268 piston cores (11), and kasten cores (2). The multicorer was an 8-tube corer built by Oktopus

GmbH weighing 500kg. The polycarbonate liners were 60 cm long with a 10 cm diameter. The piston/gravity coring system was built by Stockholm University with an inner diameter of 10 cm. Trigger weight cores also were collected during piston coring. The different coring systems enabled sediment and pore water collection from the seafloor to upwards of nine m below the seafloor (mbsf).

3.2 Core material

Sediment physical properties on gravity and piston cores were analyzed on the ship using a Geotek Multi-Sensor Core Logger (MSCL). Measurements of the gamma-ray derived bulk density, compressional wave velocity (p-wave), and magnetic susceptibility were acquired at a down core resolution of one cm. Discrete samples (2-3 per section) also were collected for sediment index property measurements (bulk density, porosity, water content and grain density). Grain density was measured using a helium displacement pycnometer on oven-dried samples. Porosity profiles were generated using the smoothed (3-pt) MSCL-derived bulk density (ρ_B) and the average grain density (ρ_g) from each core, where

$$\varphi = \frac{(\rho_g - \rho_b)}{(\rho_b - \rho_f)}, \quad (5)$$

and an assumed pore fluid density (ρ_f) of 1.024 g/cm^3.

3.3 Interstitial water collection

Pore waters were collected using Rhizon samplers (Seeberg-Elverfeldt et al., 2005; Dickens et al., 2007). Cores were cut into ~1.5 m long sections immediately on the ship deck, brought to the geochemistry laboratory, and placed on precut racks. Laboratory temperature was a near constant 22 °C. Sampling involved drilling holes through the core liner, inserting Rhizons into

292 the sediment core, and obtaining small volumes of pore water via vacuum and "microfiltration."
293 The Rhizons used were 5-cm porous flat tip male luer lock (19.21.23) with 12 cm tubing,
294 purchased from Rhizosphere Research Products (www.rhizosphere.com).
295 In total, 529 pore water samples were collected from 32 cores, which ranged from 0.16 to
296 8.43 m in length (Tbl. S2). Rhizons in gravity and piston cores typically were spaced every 20 to
297 30 cm. Because the use of rhizon sampling for collecting pore waters of deep-sea sediments
298 remains a relatively novel and engaging topic (Dickens, 2007), we discuss the procedure, as well
299 as several experiments regarding our sampling, in the supplementary information document.
300 While in the shipboard laboratory, Rhizon samples were divided into six aliquots when
301 sufficient water was available. This sample splitting led to 2465 aliquots of pore water in total,
302 which then could be examined for different species and at different laboratories. Aliquots 1, 3,
303 and 6 (below) were collected for all 32 cores.
304
305 *3.4 Interstitial water analyses*
306 The first aliquot was used to measure total alkalinity using a Mettler Toledo titrator
307 onboard *IB Oden*. Immediately after collection, pore water was diluted with milli-Q water and
308 autotitrated. Fifteen spiked samples and eight duplicates were analyzed onboard for quality
309 control. Spiked samples were created by pipetting certified reference material (Batch 135;
310 www.cdiac.ornl.gov/oceans/Dickson_CRM) into milli-Q water. Results for spiked samples and
311 duplicates are reported in Table 1.
312 The second aliquot was used to measure the $\delta^{13}C$ composition of DIC ($\delta^{13}C$-DIC). Septum
313 sealed glass vials prepared with H_3PO_4 and flushed with helium were prepared before the
314 expedition. Samples were sealed in boxes and refrigerated for the remainder of the cruise. Four

315 field duplicates, two seawater standards, and a field blank were collected, stored, and analyzed
316 with the samples. The δ^{13}C-DIC analyses were performed on a Gasbench II coupled to a MAT
317 253 Mass Spectrometer (both Thermo Scientific) at Stockholm University. The δ^{13}C-DIC is
318 reported in conventional delta notation relative to Vienna PeeDee Belemnite (VPDB). Results
319 for field duplicates and standards are reported in Table 1. Standard deviation for the analyses of
320 δ^{13}C-DIC was less than 0.1 ‰.

321 The third aliquot was used to measure dissolved sulfur and metal concentrations. Samples
322 were acid preserved with 10 µL ultrapure HNO_3. Additionally, 11 blind field duplicates and 2
323 field blanks were collected and processed in the same manner. Concentrations of Ba, Ca, Fe, Mg,
324 Mn, S, and Sr were determined on an Agilent Vista Pro Inductively Coupled Atomic Emission
325 Spectrometer (ICP-AES) in the geochemistry facilities at Rice University. Known standard
326 solutions and pore fluid samples were diluted 1:20 with 18-MΩ water. Scandium was added to
327 both standards and samples to correct for instrumental drift (emission line 361.383 nm).
328 Wavelengths used for elemental analysis followed those indicated by Murray et al. (2000).
329 Following initial analysis, an additional dilution, 1:80 with 18-MΩ water, was analyzed for Ca,
330 Mg, and S. After every 10 analyses, an International Association of Physical Sciences (IAPSO)
331 standard seawater spiked sample and a blank were examined for quality control. Relative
332 standard deviations (RSD) from stock solutions are reported in Table 1.

333 The fourth aliquot was used to measure dissolved ammonia (NH_4^+) via a colorimetric
334 method similar to that presented by Gieskes et al. (1991). Set volumes of pore water were
335 pipetted into cuvettes and diluted with milli-Q water. Two reagents were then pipetted into the
336 cuvettes. Reagent A was prepared by adding $Na_3C_6H_5O_7$, C_6H_5OH, and $Na_2(Fe(CN)_5NO)$ to
337 milli-Q water. Reagent B was prepared by dissolving NaOH in milli-Q water and adding NaClO

338 solution. Solutions were mixed and allowed to react for at least six but not more than 24 hours.
339 Solutions turned various shades of blue, which to relate to NH_4^+ concentration, and were
340 measured by absorbance at 630 nm on a Hitachi U-1100 spectrophotometer. Five point
341 calibration curves were measured before each sample set and corrected using VKI standard (QC
342 RW1; www.eurofins.dk; Table 1).

343 The fifth aliquot was used to measure dissolved phosphate (PO_4^{3-}) following the method
344 given by Gieskes et al. (1991). Remaining pore water (generally between 1 and 3mL) was added
345 to milli-Q water to a sum of 10 mL. Two reagents were added to the solution to react with PO_4^{3-}.
346 Reagent A was prepared by making three solutions: $(NH_4)_2MoO_4$, H_2SO_4, and $C_8H_4K_2O_{12}Sb_2 \bullet$
347 XH_2O were added to milli-Q water, and the solutions were added dropwise. Reagent B was
348 created with $C_6H_8O_6$. After samples were prepared, reagents A and B were added, mixed, and
349 allowed to react 30 minutes. Solutions turned various shades of blue, relating to PO_4^{3-}
350 concentration, and were measured at an absorbance of 880 nm. Five point calibration curves
351 were measured before each sample set and corrected using VKI standard (QC www.eurofins.dk;
352 Table 1).

353 For 352 pore water samples, a sixth aliquot of approximately 2 mL could be collected to
354 mix with 200 µL of a 2.5% Zn-acetate ($Zn(C_2H_3O_2)_2$) solution. Given the extremely low
355 solubility of ZnS, when such a solution is added to pore water samples, a white precipitate
356 should form in the presence of even very low H_2S concentrations (Cline, 1969; Goldhaber,
357 1974).

358 A method detection limit (MDL) for each species can be determined by the following
359 equation:

360 $$MDL = \left(\frac{C_{High} - C_{Low}}{I_{High} - I_{Low}}\right) 3\sigma \,, \qquad (6)$$

where C = concentration and I = intensity (counts per second on the ICP-AES). The MDLs were as follows: Ba = 0.01 μM, Ca = 0.08 μM, Fe = 5.9 μM, Mg = 0.22 μM, Mn = 0.24 μM, S = 1.2 μM, Sr = 0.01 μM. On all plots, for reference, we place dashed lines for values of IAPSO seawater standard (Alkalinity = 2.33 mM, Ba = 0.00 mM, Ca = 10.28 mM, Fe = 0.00 mM, Mg = 53.06 mM, Mn = 0.00 mM, S = 28.19 mM, Sr = 0.09 mM, NH_4 = 0.00 mM, HPO_4 = 0.00 mM).

4. Results

4.1 Broad conclusions

With the large number of pore water measurements (Tbl. S1), we begin with some generalities regarding results. We plot pore water concentration profiles along each transect collectively (Fig. 4-8), irrespective of coring device or water depth, although clear variance in pore water chemistry exists between stations for some dissolved species (e.g., Fe).

Most species display "smooth" concentration profiles with respect to sediment depth (Fig. 4-8). That is, concentrations of successive samples do not display a high degree of scatter. This is expected for pore water profiles in sediment where diffusion dominates (Froelich et al., 1979; Klump and Martens 1981; Schulz, 2000; Torres and Kastner, 2009; Hu et al., 2015). However, for some dissolved species whose concentrations do not appreciably change over depth (e.g., Ba^{2+} and Ca^{2+}), scatter exists beyond that predicted from analytical precision. We discuss this in detail in the supplementary information.

4.2 Alkalinity and $\delta^{13}C$ of DIC

Alkalinity concentrations increase with depth in all cores (Fig. 4-8). Moreover, in most cases, the rise is roughly linear. Across all stations on the four transects, alkalinity increases by

an average of 0.51 mM/m, although variance exists between mean gradients for each transect (Tr1 = 0.46 mM/m, Tr2 = 0.34 mM/m, Tr3 = 0.91 mM/m, and Tr4 = 0.44 mM/m) and by station along each transect. Overall, the rise in alkalinity at these 15 stations ranges from 0.30 to 0.98 mM/m. The Lomonosov Ridge station differs (Fig. 8), as alkalinity increases much greater with depth (1.86 mM/m).

Concave-down δ^{13}C-DIC profiles characterize pore waters at all stations (Fig. 4-8). The decrease in δ^{13}C-DIC is most pronounced near the seafloor. Across all stations along the four transects, pore water δ^{13}C-DIC values decrease from near zero close to the mudline at an average of -3.6 ‰/m. Again, variance in mean gradients occurs according to stations and transects (Tr1 = -3.3 ‰/m, Tr2 = -3.0 ‰/m, and Tr3 = -4.7 ‰/m). As with alkalinity, the δ^{13}C-DIC profile at the Lomonosov Ridge station differs, with values decreasing by 5.6 ‰/m, such that by eight mbsf, δ^{13}C-DIC approaches -45 ‰. In summary, a basic relationship exists between higher alkalinity and lower δ^{13}C-DIC across all stations.

4.3 Sulfur and sulfate

No sulfide was observed by smell and no ZnS precipitated in any pore water sample upon addition of Zn-acetate solution. Molar concentrations of total dissolved sulfur should, therefore, represent those of dissolved SO_4^{2-}. Along the four transects, dissolved S concentrations decrease with depth at all stations (Fig. 4-7). The total dissolved S concentrations in the shallowest samples varied from 27.3 to 30.6 mM and averaged 28.7 mM. From these “seafloor” values, concentrations decrease by an average 0.69 mM/m, again with variance according to stations and transect (Tr1 = -0.58 mM/m, Tr2 = -0.57 mM/m, Tr3 = -1.09 mM/m; and Tr4 = -0.60 mM/m). The dissolved S gradients across all stations along the CESS slope range from -0.41 to -1.13

mM/m. Total dissolved S at the Lomonosov Ridge station displays a significantly steeper decrease than any other station (-1.92 mM/m). Importantly, decreases in dissolved S are similar in magnitude to increases in alkalinity at each station examined. Indeed, the molar ratio of alkalinity change with depth to sulfur change with depth ($-\Delta Alkalinity/\Delta S$) is 0.98 (Fig. 9a).

4.4 Ammonia and phosphate

The C:N:P molar ratio of typical marine organic matter is approximately 106:16:1 (Redfield, 1958; Takahashi, 1985). Although this ratio differs for terrestrial organic carbon (perhaps closer to 134:9:1, Tian et al., 2010), dissolved HPO_4^{2-} and NH_4^+ concentrations in pore water can be used in a general sense to assess consumption of particulate organic carbon. This is because organic matter degradation releases these species to pore water (Froelich et al., 1979). Notably, concentrations of NH_4^+ and HPO_4^{2-} are near or below detection in samples immediately below the seafloor (Fig. 4-8).

Dissolved NH_4^+ profiles increase almost linearly with depth, although with slight concave-down curvature. Similar to alkalinity profiles, NH_4^+ concentrations rise with depth below the seafloor more at stations with shallower water depth (although we note an exception for Tr2). Across stations along the four transects, pore water NH_4^+ concentrations increase with depth on average by 38.69 μM/m, with a range from 11.3 to 76.1 μM/m. Along each transect, the average NH_4^+ gradients are as follows: Tr1 = 43.0 μM/m, Tr2 = 17.4 μM/m, Tr3 = 69.0 μM/m, and Tr4 = 29.0 μM/m.

By contrast, concentrations of dissolved HPO_4^{2-} in our cores typically increase, reach a subsurface maximum, and then decrease (Fig. 4-8). With available data, a more pronounced maximum generally occurs at stations with relatively shallow water depth. For example, consider

the peak in HPO_4^{2-} concentrations at four stations. At the two shallow stations, S12 (384 m) and S22 (367 m) the HPO_4^{2-} maxima are, 73 μM (1.91 m) and 18 μM (0.66 m), respectively, but at the two deeper stations, S17 (977 m) and S14 (733 m), the HPO_4^{2-} maxima are only 6.7 μM (1.76 m) and 7.1 μM (2.33 m) respectively. The station on Lomonosov Ridge (S31) has a high in HPO_4^{2-} concentration of 76 μM at 1.02 m below the mudline. In general, stations with more pronounced HPO_4^{2-} maxima also have greater increases in alkalinity with depth.

The NH_4^+, HPO_4^{2-}, and alkalinity profiles relate to one another statistically, although with distinction. All stations have a C:N ratio in pore waters much higher than the canonical Redfield Ratio of 6.625 (Fig. 10). Rather, the concentration relationship of alkalinity and ammonium ion can be expressed by a second order polynomial ($[NH_4^+] = -0.003[Alk]^2 + 0.105\ [Alk] – 0.253$; Fig. 9b) with an average molar ratio ($\Delta Alk/\Delta NH_4^+$) of 14.7, close to what might be expected for degradation of terrestrial organic carbon. Interestingly, this ratio deviates somewhat across transects, increasing at sites from Tr1, Tr3, Tr2, to the Lomonosov Ridge station. The molar ratio of alkalinity to phosphate ion ($\Delta Alk/\Delta HPO_4^{2-}$) averages 55.7 for all stations. This ratio also generally increases in cores from east to west.

4.5 Metals

At most stations, dissolved Ba^{2+} concentrations increase nonlinearly from values at or below detection limit (0.01 μM) near the seafloor to generally constant values (0.6 – 0.7 μM) within 0.8 m below the seafloor. However, at several stations, dissolved Ba^{2+} concentrations remains at or below the detection limit for all samples.

Overall, dissolved Ca^{2+}, Mg^{2+}, and Sr^{2+} concentrations decrease slightly with depth (Fig. 4-8). Across stations along the four transects, Ca^{2+} concentrations drop on average between -0.09

and -0.12 mM/m (Tr1), about -0.09 mM/m (Tr2), between -0.09 and -0.10 (Tr3), and -0.075 mM/m (Tr4). Magnesium concentrations also drop, the average change being between -0.43 and -0.48 mM/m (Tr1), between -0.27 and -1.32 (Tr2), between -0.86 and -0.94 mM/m (Tr3), and -0.467 mM/m (Tr4). Strontium concentrations decrease by an average amount of 0.3 μM/m, considering all stations along the four transect stations (Tr1 = 0.5 μM/m, Tr2 = 0.3 μM/m, Tr3 = 0.1 μM/m, and Tr4 = 0.1 μM/m). The station on Lomonosov Ridge again stands apart. At this location, the decreases in dissolved Ca, Mg, and Sr are 0.27 mM/m, 1.24 mM/m, and 0.50 μM/m, respectively.

The profiles of dissolved Mn and Fe are complicated in terms of location. Generally, profiles show a broad rise in concentrations within the upper sediment and a subsequent drop in concentrations at deeper depth. Some stations have a maxima in dissolved Mn (Stations S12 (135 μM at 5 m), S28 (66 μM at 3.1 m), and Lomonosov Ridge (86 μM at 1.3 m), where concentrations decrease below. At other stations, however, Mn concentrations still appear to be increasing at the lowest depth. Iron concentrations are generally below the detection limit at or near the mudline, and begin increasing around 2.5 – 3.5 m, reaching concentrations upward of 20 μM.

5. Discussion

5.1 Fidelity of rhizon pore water measurements

Researchers have employed multiple methods to extract pore waters from marine sediments over the last few decades, but the rhizon technique remains relatively novel (e.g., Seeberg-Elverfeldt et al., 2005; Dickens et al., 2007; Pohlman et al., 2008). Several studies have questioned the accuracy and precision of analyses obtained through this approach (e.g., Schrum

et al., 2012; Miller et al., 2014). Two experiments conducted during the SWERUS-C3 Leg 2 Expedition using the Rhizons suggest that part of the problem concerns the timing and location of sampling (Supplementary Materials). Notably, however, as clearly documented in previous works (Seeberg-Elverfeldt et al., 2005; Dickens et al., 2007; Pohlman et al., 2008), rhizon sampling can lead to "smooth" concentration profiles for multiple dissolved species, including alkalinity (Fig. 4-8).

Concerns about rhizon sampling may be valid for dissolved components when concentration gradients are very low. For example, Schrum et al. (2012) stressed alkalinity differences between samples collected at similar depth using rhizon sampling and conventional squeezing. However, the total alkalinity range in this study was between 1.6 and 2.6 mM, and typical differences were 0.06 mM. A similar finding occurs in the dissolved Ca^{2+} and Ba^{2+} profiles of this study, where the range in values is small and adjacent samples deviate by more than analytical precision (Tbl. 1, Fig. S3). However, when the signal to noise ratio becomes high, as true with most dissolved components at most stations (Fig. 4-8), the rhizon sampling renders pore water profiles with well-defined concentration gradients that can be interpreted in terms of chemical reactions and fluxes.

5.2 General absence of methane

Direct measurements of dissolved CH_4 in deep-sea sediment are complicated (Claypool and Kvenvolden 1983). During core retrieval and depressurization, significant CH_4 loss can occur from pore space (Dickens et al., 1997). Moreover, in sediments containing high CH_4 concentrations and recovered through piston coring, such gas release typically generates sub-

horizontal cracks that span the core between the liner. No such cracks were documented in any of the cores.

Excluding Station St31 on the southern Lomonosov Ridge (discussed below), there is no indication of a shallow SMT. Interstitial water sulfur concentrations do not drop below 22.8 mM within the upper 8 m. In fact, calculated downward SO_4^{2-} fluxes, as inferred from sulfur concentration gradients (Tbl. 2) range from -1.8 to -6.2 mol/m^2-kyr for all stations except Station S31. For comparison, a site with a near seafloor temperature of 2 °C (Fig. S2) and porosities similar to those measured (Fig. S1), an SMT at 6.0 mbsf would imply a SO_4^{2-} flux of -40 mol/m^2-kyr.

Given the lack of HS^- and the measured pH at Station S33 (Fig. S2), alkalinity should closely approximate HCO_3^- concentrations (Equation 4). Estimated HCO_3^- fluxes ($J HCO_3^-$) do not exceed 6.8 mol/m^2-kyr at any station east of the Lomonosov Ridge (Tbl. 2). For comparison, at sites with abundant CH_4 at depth, $J HCO_3^-$ generally exceeds 30 mol/m^2-kyr above the SMT (Tbl. 2). These extreme fluxes arise because methanogenesis in deeper sediment drives an upward flux of HCO_3^- (Fig. 3), and because AOM contributes additional HCO_3^- and HS^- to pore water at the SMT (Eqn. 1).

The δ^{13}C-DIC values of pore water decrease with depth at all stations, almost in concert with the rise in alkalinity, implying no CH_4 production because methanogenesis would increase δ^{13}C-DIC values (Fig. 9c; Whiticar, 1999). Other than Station S31, the lowest value of δ^{13}C-DIC is -25.23 ‰ at 5.5 m at Station S22 (Fig. 6). This is interesting because a series of microbial reactions utilizing particulate organic matter (POM) can lead to higher alkalinity and lower δ^{13}C-DIC values in pore water. The most important of these reactions is organoclastic sulfate reduction (OSR), which can be expressed as (Berner, 1980; Boudreau and Westrich, 1984):

521 $$2CH_2O + SO_4^{2-} \rightarrow H_2S + 2HCO_3^-\ , \quad (7)$$

522 Notably, this reaction has a 2:1 relationship between C and S fluxes, rather than the 1:1 ratio of
523 AOM (Eqn. 1).

524 As emphasized previously, methane-charged sediment sequences do occur on continental
525 slopes in the Arctic. Of particular interest to this study are locations in the Beaufort Sea, where
526 indications for gas hydrate manifest on seismic profiles (Grantz et al., 1976; Grantz et al., 1982;
527 Weaver and Stewart, 1982; Hart et al., 2011; Phrampus et al., 2014), and pore water profiles
528 have been generated using shallow piston cores (Coffin et al., 2013). Striking contrasts exist
529 between pore water profiles of the Beaufort Sea and those of the CESS (Tbl. 2). In the Beaufort
530 Sea, there are moderate to high downward SO_4^{2-} and upward CH_4 fluxes (1.9 to 154.8 mol/m^2-
531 kyr), shallow SMTs (6.29 to 1.06 mbsf), high DIC fluxes between the SMT and the mudline
532 (46.3 to 242.6), and negative δ^{13}C-DIC values at SMT's (≈ -20‰).

533

534 *5.3 Special case "Lomonosov Ridge station"*

535 Station 31 on the Lomonosov Ridge (Fig. 8) differs from all other stations examined in
536 this study. Here, pore water chemistry profiles hint at CH_4 in pore space within shallow
537 sediment. Extrapolation of the dissolved sulfur profile suggests an SMT at approximately 14
538 mbsf. Such a depth lies within the range common for locations with AOM (D'Hondt et al.,
539 2002), notably including well studied sites on Blake Ridge (Borowski et al., 1999). Similar to
540 some sites with CH_4, the δ^{13}C-DIC values become very "light"; indeed, the value at the base of
541 the core, -43.5‰, almost necessitates CH_4 oxidation within shallow sediment. Comparably steep
542 alkalinity (1.6 mM/m) and NH_4 gradients (60.4 μM/m) also characterize most sites with CH_4
543 near the seafloor. However, there is an issue concerning reduced sulfur, which is a product of

AOM (Eqn. 1). If AOM was occurring at ~13.9 mbsf, one might expect evidence for HS^- migrating from below (Fig. 3). No ZnS precipitated in pore waters of this core upon addition of ZnAc.

A comparison of published DIC fluxes, SO_4^{2-} fluxes, and SMT depths (Tbl. 2) reveals fluxes decrease exponentially with SMT depth (Fig. 11). In fact, a fundamental relationship exists when one considers that upward CH_4 fluxes control the SMT depth (Eqn. 1; Fig. 3). The modest SO_4^{2-} flux (-13.9 mol/m^2-kyr) and alkalinity flux (11.3 mol/m^2-kyr) estimated for the Lomonosov Ridge station conform to those expected for an SMT at about 14 mbsf. For example, Hensen et al. (2003) calculated a SO_4^{2-} flux of -14.7 mol/m^2-kyr for a site with an SMT at 14 mbsf in the Argentine Basin, and Berg (2008) calculated a SO_4^{2-} flux of -8.05 mol/m^2-kyr for a site with an SMT at 16 mbsf along the Costa Rica Margin.

5.4 Other chemistry

Microbial communities preferentially utilize the most energetically favorable oxidant available, which leads to a characteristic sequence of reactions in marine sediment (Froelich et al., 1979; Berner, 1980; D'Hondt et al., 2004; Miller et al., 2012). With increasing depth below the seafloor, these reactions are: aerobic respiration, denitrification, manganese oxide reduction, iron oxide reduction, SO_4^{2-} reduction, and finally methanogenesis. Importantly, depths dominated by these reactions generally depend on the supply of POM to the seafloor, and these reactions impact pore water chemistry.

Many of the cores collected along the CESS slope appear to terminate in the zone of metal oxide reduction. This is because, at most stations, Mn and Fe profiles are still increasing at the bottom of the sampled interval (Fig. 4-8) which may be due to dissimilatory Mn- and Fe-

oxide reduction. However, Mn in particular may be more complicated. März et al., (2011) find evidence from Mn profiles along the southern Mendeleev Ridge which may reflect diagenetic remobilization and diffusion from deeper sediments. The relatively deep depths of metal oxide reduction nevertheless, are consistent with a relatively low input of POM to the seafloor, and generally contrast with sites of high CH_4 concentrations in shallow sediment. From a simple perspective, there may be insufficient POC to drive methanogenesis near the seafloor.

The station on the Lomonosov Ridge again stands apart. Here, Mn and Fe concentrations reach maxima at 1.3 mbsf and 0.5 mbsf, respectively, and decrease below. This is likely due to Mn and Fe produced during dissimilatory oxide reduction occurring below consumption. Thus, the Lomonosov Ridge site appears to have higher organic turnover and possibly more organic burial than all the other locations.

Presumably, organic matter ultimately mineralized as CH_4 in Arctic sediments is produced during warm periods. Before the opening of the Fram Strait, ocean water stratification was likely pronounced, causing widespread anoxia. Bottom water anoxia created optimal conditions for organic matter preservation. During the current interglacial, however, organic matter deposition in the ESM is seasonal and small. The relationship of alkalinity to ammonia in Figure 10 exceeds the Redfield ratio of the average marine organic matter. Therefore, the source of much of the organic matter on the continental slope may be terrestrial rather than marine.

5.5 Signatures of AOM and OSR

Some authors have used changes in DIC and SO_4^{2-} concentrations between the seafloor and the SMT to infer the relative importance of AOM and OSR in marine sediments (Kastner et al. 2008b; Luo et al. 2013; Hu et al. 2015). This idea can be expressed by comparing

590 $\Delta(DIC+Ca^{2+}+Mg^{2+})$ and ΔSO_4^{2-}, where Ca^{2+} and Mg^{2+} are included to account for loss of DIC
591 via carbonate precipitation (other authors, such as Snyder et al., 2007 and Wehrmann et al.,
592 (2011) use fluxes instead of concentrations). The rationale lies in the fact that the C:S ratio for
593 AOM is 1:1 (Eqn. 1), whereas the C:S ratio for OSR is 2:1 (Eqn. 8). However, this approach
594 neglects two considerations: (1) changes in concentration do not directly relate to fluxes, because
595 of differences in diffusivities of various ionic species, and, (2) a flux of HCO_3^- from below the
596 SMT can augment the DIC produced from AOM or OSR at or above the SMT (Dickens and
597 Snyder, 2009). Thus, changes in alkalinity relative to SO_4^{2-} often exceed 1:1, even at locations
598 completely dominated by AOM (Chatterjee et al., 2011).
599 Rather than just comparing changes in C:S molar ratios, to interrogate the importance of
600 the two reactions, one might also incorporate δ^{13}C-DIC value. This is because δ^{13}C-DIC values
601 and the depth of DIC production differ considerably for AOM, OSR and methanogenesis at
602 many locations. We generate a figure expressing these relationships at multiple sites (Fig. 12),
603 where the y-axis is:

$$\frac{\Delta(DIC + Ca^{2+} + Mg^{2+})}{\Delta(SO_4^{2-})}, \quad (8)$$

604 and the x-axis is: DIC*δ^{13}C-DIC. The C:S ratios of dissolved species lie above 1:1 at most
605 locations, regardless of whether CH_4 exists in shallow sediment. However, sites with CH_4 have
606 considerably more negative DIC*δ^{13}C-DIC values. Notably, all CESS stations, except S31 on the
607 Lomonosov Ridge, have modest DIC*δ^{13}C-DIC values.
608 In summary, from general pore water considerations as well as from comparisons to pore
609 water profiles at other locations, sediments along the CESS continental slope do not contain
610 significant CH_4 in shallow sediment. Implicit in this finding is that sediment sequences along the
611 CESS lack large-scale gas hydrate. As models for gas hydrate occurrence in the Arctic (Fig. 1)

612 correctly predict gas hydrate in several regions (e.g., Kvenvolden and Grantz, 1990; Max and
613 Lowrie, 1993; Max and Johnson, 2012), our findings prompt an interesting question: why are
614 predictions so markedly wrong for the CESS?
615
616 *5.6 Possible explanations for methane absence*
617 To understand the absence of gas hydrates on the CESS, one needs to consider the
618 generalities of gas hydrate occurrence in marine sediment. There are two basic conditions for gas
619 hydrate on continental slopes (Kvenvolden, 1993; Dickens, 2001). The first is the "potential
620 volume", or the pore space where physiochemical conditions (e.g., temperature, pressure,
621 salinity, sediment porosity) are amenable to gas hydrate formation. As stressed in previous
622 works, the CESS, with cold bottom water and a low geothermal gradient, has a relatively large
623 volume of sediment with appropriate gas hydrate stability conditions (Stranne et al., 2016). The
624 second is the "occupancy", or the fraction of sediment pore space with sufficient CH_4 to
625 precipitate gas hydrate. The short answer is that environmental conditions on the CESS are
626 highly conducive for gas hydrate, but there is little CH_4.
627 It is also important to recognize how diffusive systems operate in marine sediment.
628 Hundreds of pore water profiles have been generated during scientific ocean drilling expeditions,
629 including scores into CH_4 charged sediment sequences. These profiles almost universally show
630 connectivity of pore water chemistry over hundreds of meters (Fig. 3). This occurs because,
631 given sufficient permeability and time, diffusive fluxes transport species from intervals of high
632 concentration to intervals of low concentration. Hence, unless some impermeable layer exists in
633 the sediment sequence, even CH_4 at depth impacts near seafloor concentrations. Indeed, ODP
634 Leg 164 on the outer Blake Ridge wonderfully shows this phenomenon. The uppermost gas

635 hydrate in sediment in this region probably lies at about 190 mbsf; nonetheless, its presence can
636 be observed in shallow pore water profiles, because the flux of CH_4 from depth drives AOM near
637 the seafloor (Borowski et al., 1999; Dickens, 2001).

638 For these reasons, bubble-mediated CH_4 transport from widespread gas hydrates
639 occurring between transects is unlikely. No major physiographic provinces exist between
640 transects (Fig. 1 and 2). All major sedimentary regions within the field area are included within
641 the transects. All observed large-scale gas hydrate accumulations with bubble-mediated CH_4
642 transport also have significant CH_4 diffusion. This is because sediment sequences with gas
643 hydrate have gas hydrate formation, gas hydrate dissociation, and gas hydrate dissolution all co-
644 occurring (Dickens, 2003). The pore water gradients between the top of the gas hydrate stability
645 zone and the seafloor occur due to steady-state formation and dissolution. Therefore, it is
646 unlikely that widespread gas hydrate accumulations exist and are somehow only venting in small
647 localized regions. Therefore, assuming that an impermeable layer does not exist in the upper few
648 hundreds of meters of sediment on slopes of the CESS, the lack of gas hydrates and CH_4
649 suggests either insufficient POC to generate CH_4, or substantial loss of CH_4 over time.

650 The accumulation of POC on CESS slopes may be relatively low over the Plio-
651 Pleistocene, an amount too small to drive methanogenesis. With low POC inputs, other microbial
652 reactions can exhaust the organic matter needed for methanogenesis. This may, in fact, explain
653 why the pore water chemistry suggests that metal-oxide reduction dominates the geochemical
654 environment at most stations on the CESS. Additionally, Ba^{2+} concentrations do not provide
655 evidence for bio-barite dissolution. Without further investigation, we can offer three possibilities
656 as to why this might occur: (1) significant sea-ice concentrations, both at present-day and during
657 past glacial intervals, greatly diminishes primary production within the water column, one may

ask, however, why this process would hinder production above CESS sediments and not above other Arctic provinces with demonstrated gas hydrate accumulations; (2) the extremely broad continental shelf prevents large accumulations of terrestrial organic rich sediment from reaching the slope, the enormous continental shelf, is indeed, the primary dissimilarity to other Arctic margins; or (3) highly variable sediment accumulation, perhaps corresponding to glacial-interglacial oscillations, creates a situation where organic matter can be consumed during intervals of low deposition. In the latter case, large glaciers in the past may have physically removed sediment (and organic matter) from the slope (Jakobsson et al., 2014).

There is also the issue of POC that likely accumulated in the Cretaceous through early Eocene (Sluijs et al., 2006; Backman et al., 2009). In theory, organic-rich sediment accumulated around the Arctic during this time, which should have generated CH_4. This CH_4 could either be too deeply buried to migrate into the modern GHSZ or has been lost in the intervening time.

6. Conclusions

Leg 2 of the SWERUS-C3 expedition recovered sediments and pore waters from numerous stations across the CESS continental slope. These stations extend from Wrangel Island to the New Siberian Islands, and give information from a climatically sensitive but highly inaccessible area.

In an effort to understand CH_4 cycling on the CESS continental slope, we generated detailed pore water profiles of multiple dissolved constituents at the stations. The pore water profiles are coherent and interpretable, and give a general view: most stations have low SO_4^{2-} and HCO_3^- fluxes (<6.2 and 6.8 mol/m^2-kyr respectively), a moderate decrease in δ^{13}C-DIC values with depth (-3.6‰/m average), no dissolved H_2S, moderate rise in HPO_4^{2-} and NH_4

concentrations, and slightly decreasing Ca^{2+}, Mg^{2+}, and Sr^{2+} concentrations. Except for one station on the Lomonosov Ridge, metal oxide reduction appears to be the dominant geochemical environment affecting shallow sediment, and there is no evidence for upward diffusing CH_4. These results strongly suggest that gas hydrates do not occur on slopes of the CESS. This directly conflicts with multiple publications, which have assumed large quantities of CH_4 and gas hydrate in the region. It is possible that CH_4 and gas hydrate occur where the Lomonosov Ridge intersects the CESS.

The contradiction between models for gas hydrate in the region and actual data may arise for two basic reasons. First, in relatively recent geological times, insufficient POC accumulates along the slope to form CH_4 and gas hydrates; second, CH_4 generated from POC deposited in older geological times is too deeply buried or has been lost.

Acknowledgments. The authors would like to thank the SWERUS-C3 Leg 2 crew as well as reviewers.

Table List

Table 1 - QA/QC

Table 2 - Published and Calculated Fluxes

a = Coffin et al., 2013; b = Personal Communication; c = Coffin et al., 2007; d = Coffin et al., 2006; e = Coffin et al., 2008; f = Hamdan et al., 2011 and Coffin et al., 2014; g = Dickens and Snyder, 2009; h= Snyder et al., 2007; i = Mountain et al., 1994; j = Lin et al., 2006; k = Berelson et al., 2005; l = Hensen et al., 2003; m = Dickens, 2001; n = Geprags et al., 2016; o = Claypool et al., 2006; p = Keigwin et al., 1998; q = Berg, 2008; r = Borowski et al., 2000; s = D'Hondt et al., 2002; t = D'Hondt et al., 2004; u = Torres et al., 2009; v = Burns, 1998; w = Kastner et al., 2008; x = Paull et al., 1996; y = Flood et al., 1995; z = Wefer et al., 1998; 1 = Prell et al., 1998; 2 = Takahashi et al., 2011; 3 = Riedel et al., 2006; 4 = Tamaki et al., 1990; 5 = Lyle et al., 1997; 6 = Moore et al., 2001; 7 = Kimura et al., 1997; 8 = Suess et al., 1988; 9 = D'Hondt et al., 2003. ‡ = Calculated from published material.

Figure Captions

Figure 1. Generalized Arctic map with background from GeoMapApp (http://www.geomapapp.org; Ryan et al., 2009). Observed sulfate-methane transitions during the MITAS 1 expedition shown in black diamonds (Coffin et al., 2013) and Arctic Coring Expedition (ACEX) shown as red squares (Backman et al., 2009).

Figure 2. Bathymetric map of Eurasian Arctic showing the overall cruise track of Leg 2 along with the four transects and coring locations. Multicores shown as yellow triangles, gravity and piston cores as white stars, and the ship trackline as gray line from Barrow, Alaska.

Figure 3. Idealized pore water concentration profiles for high and low upward methane flux. Discrete data points for sites 722 (Arabian Sea; Seifert and Michaelis, 1991; D'Hondt et al., 2002) and 1230 (offshore Peru; Donohue et al., 2006) are given as reference.

Figure 4. Transect 1. results. IAPSO standard seawater (black dotted line) shown for comparison.

Figure 5. Transect 2. results. IAPSO standard seawater (black dotted line) shown for comparison.

Figure 6. Transect 3. results. IAPSO standard seawater (black dotted line) shown for comparison.

Figure 7. Transect 4. results. IAPSO standard seawater (black dotted line) shown for comparison.

Figure 8. Lomonosov Ridge Station results. IAPSO standard seawater (black dotted line), and representative stations from the four transects shown for comparison.

Figure 9. Relationship of (a) sulfate change (ΔSO_4^{2-}) and carbonate corrected alkalinity change ($\Delta Alk+Ca^{2+}+Mg^{2+}$) following 2:1 ratio; (b) the second order polynomial association of NH_4^+ to Alkalinity; and (c) decreasing δ^{13}C-DIC values with alkalinity increase. Methane charged sites (1230, 1426, and 1427; 1230, Shipboard Scientific Party, 2003; 1426 and 1427, Expedition Scientists, 2014) given for comparison.

Figure 10. C:N:P ratio indirectly shown with $\Delta Alk/\Delta NH_4^+$ and $\Delta Alk/\Delta HPO_4^{2-}$. Several global sites, 994, 995, 997, 1059, 1225, 1230, 1426, 1427, and 1319 (994-997, 1059, Borowski et al., 2000; 1225 and 1230, Shipboard Scientific Party, 2003; 1426 and 1427, Expedition Scientists, 2014) given for comparison. Blue marginal distribution curves show global distribution while red gives CESS stations (this project). CESS pore waters have higher C:N and lower C:P than comparative sites.

Figure 11. Bicarbonate (HCO_3^-) and sulfate (SO_4^{2-}) flux exponential relationship with SMT depth for all sites listed in Table 2.

Figure 12. Ratio of carbonate corrected alkalinity change ($\Delta Alk+Ca^{2+}+Mg^{2+}$) and sulfate change ($\Delta SO_4^{2-}$) to the product of DIC and δ^{13}C-DIC value (AT13-2 and KC151, Kastner et al., 2008a;

PC02-PC14, Coffin et al., 2008; 994-997, 1059, Borowski et al., 2000; Paull et al., 2000; 1326 and 1329, Torres and Kastner, 2009; GC233 and GB425, Hu et al., 2010; D-5 – D-8 and D-F, Hu et al., 2015; C9-C19, Luo et al., 2013; PC-07, Smith and Coffin, 2014; 1230, Shipboard Scientific Party, 2003; 1244 and 1247, Claypool et al., 2006; 1305 and 1306, Party, 2005) including global sites for comparison) showing the paucity of methane charged sites actually reaching 1:1 C:S ratio. Error bars are one sigma. CESS plotted pore waters substitute alkalinity for DIC. With the absence of sulfide, DIC and alkalinity should be roughly equivalent in these pore waters. CESS locations use the same symbols as previous figures.

766 **References:**

767 Aagaard, K., Coachman, L. K., and Carmack, E. C.: On the halocline of the Arctic Ocean, Deep
768 Sea Res., 28, 529-545, 1981.

769 Aagaard, K. and Carmack, E. C.: The role of sea ice and other fresh water in the Arctic
770 Circulation, J. Geophys. Res., 94, 14485–14498, 1989.

771 Aharon, P. and Fu, B.: Microbial sulfate reduction rates and sulfur and oxygen isotope
772 fractionations at oil and gas seeps in deepwater Gulf of Mexico. Geochimica et
773 Cosmochimica Acta, 64(2), pp.233-246, 2000.

774 Alekseev, M. N.: Paleogeography and geochronology in the Russian eastern arctic during the
775 second half of the quaternary, Quatern. Int., 41/42, 11–15, 1997.

776 Alperin, M. J., Reeburgh, W. S., and Whiticar, M. J.: Carbon and hydrogen isotope fractionation
777 resulting from anaerobic methane oxidation, Global Biogeochem. Cy., 2, 279-288, 1988.

778 Andreassen, K., Hogstad, K., and Berteussen, K. A.: Gas hydrate in the southern Barents Sea
779 indicated by a shallow seismic anomaly, First Break, 8, 235–245, 1990.

780 Andreev, A. A., Grosse, G., Schirrmeister, L., Kuznetsova, T. V., Kuzmina, S. A., Bobrov, A.
781 A., Tarasov, P. E., Novenko, E., Yu., Meyer, H., Derevyagin, A., Yu., Kienast, F.,
782 Bryantseva, A., and Kunitsky, V. V.: Weichselian and Holocene palaeoenvironmental
783 history of the Bol'shoy Lyakhovsky Island, New Siberian Archipelago, Arctic Siberia.
784 Boreas 38, 72–110, 2009.

785 Archer, D. E.: Methane hydrate stability and anthropogenic climate change, Biogeosciences, 4,
786 993-1057, 2007.

787 Archer, D.: A model of the methane cycle, permafrost, and hydrology of the Siberian continental
788 margin, Biogeosciences, 12 (10), 2953–2974, 2015.

Augstein, E.: Die Expedition ARCTIC'96 mit FS" Polarstern"(ARK XII) mit der Arctic Climate System Study (ACSYS); The expedition ARCTIC'96 of RV" Polarstern"(ARK XII) with the Arctic Climate System Study (ACSYS). Berichte zur Polarforschung (Reports on Polar Research), 234, 1997.

Backman, J., and Moran, K.: Expanding the Cenozoic paleoceanographic record in the Central Arctic Ocean: IODP Expedition 302 Synthesis: Central European Journal of Geosciences, 1, 2, 157-175, 2009.

Bakhmutov, V., Whitledge, T., Wood, K. and Ostrovskiy, A.: Report on the execution of marine research in the Bering Strait, East Siberian and the Chukchi Sea by the Russian-American Expedition under the program of" RUSALCA" during the period from 23 August through 30 September, 2009.

Barnes, R. O. and Goldberg, E. D.: Methane production and consumption in anoxic marine sediments, Geol. 4, 297–300, 1976.

Beaudoin, Y. C., Waite, W., Boswell, R., and Dallimore, S. R.: Frozen Heat: A UNEP Global Outlook on Methane Gas Hydrates. Volume 1. UN. Environ. Programme, GRID-Arendal, 2014.

Berelson, W. M., Prokopenko, M., Sansone, F. J., Graham, A. W., McManus, J. and Bernhard, J. M.: Anaerobic diagenesis of silica and carbon in continental margin sediments: discrete zones of TCO 2 production. Geochimica et cosmochimica acta, 69 (19), 4611-4629, 2005.

Berg, P., Risgaard-Petersen, N., and Rysgaard, S.: Interpretation of measured concentration profiles in sediment pore water, Limnol. Oceanogr., 43, 1500-1510, 1998.

811 Berg, R.D.: Diffusional methane fluxes within continental margin sediments and depositional
812 constraints on formation factor estimates, ProQuest, 2008.
813 Berner, R. A.: Diagenetic models of dissolved species in the interstitial waters of compacting
814 sediments, Am. J. Sci., 275, 88–96, 1975.
815 Berner, R. A.: Stoichiometric models for nutrient regeneration m anoxic sediment?, Limnology,
816 22, 781-786, 1977.
817 Berner, R. A.: Early Diagenesis: A Theoretical Approach, Princeton University Press, Princeton,
818 N. J., 1980.
819 Bhatnagar, G., Chatterjee, S., Chapman, W. G., Dugan, B., Dickens, G. R., and Hirasaki G. J.:
820 Analytical theory relating the depth of the sulfate-methane transition to gas hydrate
821 distribution and saturation, Geochem. Geophy. Geosy., 12, 1-21, 2011.
822 Biastoch, A., Treude, T., Ruepke, L. H., Riebesell, U., Roth, C., Burwicz, E. B., Park, W., Latif,
823 M., Boening, C. W., Madec, G., and Wallmann, K.: Rising Arctic Ocean temperatures
824 cause gas hydrate destabilization and ocean acidification, Geophys. Res. Lett., 38, 1-5,
825 2011.
826 Boetius, A., Ravenschlag, K., Schubert, C. J., Rickert, D., Widdel, F., Gieseke, A., Amann, R.,
827 Jørgensen, B. B., Witte, U. and Pfannkuche, O.: A marine microbial consortium
828 apparently mediating anaerobic oxidation of methane, Nature, 407, 623-626, 2000.
829 Borowski, W. S., Paull, C. K., and Ussler III, W.: Marine porewater sulfate profiles indicate in
830 situ methane flux from underlying gas hydrate, Geol. 24, 655– 658, 1996.
831 Borowski, W. S., Paull, C. K., and Ussler W. III: Global and local variations of interstitial sulfate
832 gradients in deepwater, continental margin sediments: Sensitivity to underlying methane
833 and gas hydrates, Mar. Geol., 159, 131–154, 1999.

834 Borowski, W. S., Hoehler, T. M., Alperin, M. J., Rodriguez, N. M. and Paull, C.K.: Significance
835 of anaerobic methane oxidation in methane-rich sediments overlying the Blake Ridge gas
836 hydrates. In Proceedings of the ocean drilling program, scientific results (Vol. 164, pp.
837 87-99, 2000).
838 Borowski, W. S., Cagatay, N., Ternois, Y., and Paull, C. K.: Data Report: carbon isotopic
839 composition of dissolved CO2, CO2 gas, and methane, Blake –Bahama Ridge and
840 Northeast Bermuda Rise, ODP Leg 172, In: Keigwin, L. D., Rio, D., Acton, G. D.,
841 Arnold, E. (Eds.), Proceedings of the ODP. Scientific Results (College Station, TX), vol.
842 172, 1–16, 2001.
843 Boudreau, B. P. and Westrich, J. T.: The dependence of bacterial sulfate reduction on sulfate
844 concentration in marine sediments, Geochimica Cosmochimica Acta, 48, 2503–2516,
845 1984.
846 Buffett, B. and Archer, D.: Global inventory of methane clathrate: sensitivity to changes in the
847 deep ocean, Earth Planet. Sc. Lett., 227, 185–199, 2004.
848 Burns, S.J.: Carbon isotopic evidence for coupled sulfate reduction-methane oxidation in
849 Amazon Fan sediments. Geochimica et Cosmochimica Acta, 62(5), 797-804, 1998.
850 Carcione, J. M. and Tinivella, U.: Bottom-simulation reflectors: Seismic velocities and AVO
851 effects, Geophysics, 65, 54–67, 2000.
852 Chatterjee, S., Dickens, G. R., Bhatnagar, G., Chapman, W. G., Dugan, B., Snyder, G. T., and
853 Hirasaki, G. J.: Pore water sulfate, alkalinity, and carbon isotope profiles in shallow
854 sediment above marine gas hydrate systems: A numerical modeling perspective, J.
855 Geophys. Res-Sol. Ea., 116, 1-25, 2011.

856 Chand, S., Mienert, J., Andreassen, K., Knies, J., Plassen, L., and Fotland, B.: Gas hydrate
857 stability zone modelling in areas of salt tectonics and pockmarks of the Barents Sea
858 suggests an active hydrocarbon venting system, Mar. Petrol. Geol., 25, 625–636, 2008.
859 Clark, D. L.: Early history of the Arctic Ocean, Paleoceanography, 3, 539-550, 1988.
860 Claypool, G. E. and Kvenvolden, K. A.: Methane and other hydrocarbon gases in marine
861 sediment, Annu. Rev. Earth Pl. Sc., 11, 299-327, 1983.
862 Claypool, G. E., Milkov, A. V., Lee, Y. J., Torres, M. E., Borowski, W.S., and Tomaru, H.:
863 Microbial Methane Generation and Gas Transport in Shallow Sediments of an
864 Accretionary Complex, Southern Hydrate Ridge (ODP Leg 204), Offshore Oregon USA,
865 In: Trehu, A.M., Bohrmann, G., Torres, M.E., Colwell, F.S. (Eds.), In Proceedings of the
866 ODP, Scientific Results. Ocean Drilling Program, College Station, Texas, 2006.
867 Cline, J. D.: Spectrophotometric determination of hydrogen sulfide in natural waters, Limnol.
868 Oceanogr., 14, 454-458, 1969.
869 Coffin, R. B., Pohlman, J. W., Gardner, J., Downer, R., Wood, W., Hamdan, L., Walker, S.,
870 Plummer, R., Gettrust, J., and Diaz, J.: Methane hydrate exploration on the mid Chilean
871 coast: a geochemical and geophysical survey, J. Petrol. Sci. Eng., 56, 32-41, 2007.
872 Coffin, R., Hamdan, L., Pohlman, J., Wood, W., Pecher, I., Henrys, S., Greinert, J., and Faure,
873 K.: Geochemical characterization of concentrated gas hydrate deposits on the Hikurangi
874 Margin, New Zealand. Preliminary Geochemical Cruise Report. NRL/MR/ 6110-07,
875 2007.
876 Coffin, R. B., Hamdan, L. J., Plummer, R., Smith, J., Gardner, J., Hagen, R., and Wood, W.:
877 Analysis of Methane and Sulfate Flux in Methane-charged Sediments from the
878 Mississippi Canyon, Gulf of Mexico, Mar. Petrol. Geol., 25, 977–987, 2008.

879 Coffin, R. B., Plummer, R. B., Yoza, B., Larsen, R. K., Millholland, L. C., and Montgomery, M.
880 T.: Spatial variation in shallow sediment methane sources and cycling on the Alaskan
881 Beaufort Sea Shelf/Slope, Mar. Petrol. Geol., 45, 186-197, 2013.
882 Coffin, R. B., Hamdan, L. J., Smith, J. P., Rose, P. S., Plummer, R. E., Yoza, B., Pecher, I. and
883 Montgomery, M.T.: Contribution of vertical methane flux to shallow sediment carbon
884 pools across Porangahau ridge, New Zealand. Energies, 7 (8), 5332-5356, 2014.
885 Collett, T.S.: Energy resource potential of natural gas hydrates, AAPG Bull., 86, 1971–1992,
886 2002.
887 Collett, T. S., Lee, M. W., Agena, W. F., Miller, J. J., Lewis, K. A., Zyrianova, M. V., Boswell,
888 R., and Inks, T. L.: Permafrost associated natural gas hydrate occurrences on the Alaska
889 North Slope, Mar. Petrol. Geol., 28, 279-294, 2010.
890 D'Hondt, S., Rutherford, S., and Spivack, A.J.: Metabolic activity of subsurface life in deep-sea
891 sediments, Science, 295, 2067-2070, 2002.
892 D'Hondt, S. L., Jørgensen, B. B., Miller, D. J., and Shipboard Scientific Pary: Proceedings of the
893 Ocean Drilling Program, Initial Reports Volume 201, 2003.
894 D'Hondt, S., Jørgensen, B. B., Miller, D. J., Batzke, A., Blake, R., Cragg, B. A., Cypionka, H.,
895 Dickens, G. R., Ferdelman, T., Hinrichs, K. U. and Holm, N.G.: Distributions of
896 microbial activities in deep subseafloor sediments. Science, 306 (5705), 2216-2221,
897 2004.
898 Danyushevskaya, A., Yashin, D. S., and Kirillow, O. V.: Geochemical patterns of distribution of
899 organic carbon in the bottom sediments of Arctic seas, Oceanology, 20, 183-188, 1980.
900 Darby, D. A., Naidu, A. S., Mowatt, T. C., and Jones, G.: Sediment composition and
901 sedimentary processes in the Arctic Ocean. In: Y. Herman (Editor), The Arctic Seas:

902 Climatology, Oceanography, Geology and Biology, Van Nostrand Reinhold, New York,
903 657-720, 1989.
904 Dehairs, F., Chesselet, R., and Jedwab, J.: Discrete suspended particles of barite and the barium
905 cycle in the ocean, Earth Planet. Sci. Lett., 49, 528–550, 1980.
906 Devol, A. H.: Are high rates of sulphate reduction associated with anaerobic oxidation of
907 methane?, Nature, 291, 407-408, 1981.
908 Dickens, G. R., Paull, C. K. and Wallace, P.: Direct measurement of in situ methane quantities in
909 a large gas hydrate reservoir. Nature, 385, 426-428, 1997.
910 Dickens, G. R.: Sulfate profiles and barium fronts in sediment on the Blake Ridge. Present and
911 past methane fluxes through a large gas hydrate reservoir, Geochim. Cosmochim. Ac.,
912 65, 529-543, 2001.
913 Dickens, G. R.: Rethinking the global carbon cycle with a large, dynamic and microbially
914 mediated gas hydrate capacitor. EPSL, 213 (3), 169-183, 2003.
915 Dickens, G. R.: Rhizon sampling of pore waters on scientific drilling expeditions: an example
916 from the IODP Expedition 302, Arctic Coring Expedition (ACEX). Sci. Drill 4, 22–25,
917 2007.
918 Dickens, G.R. and Snyder, G.T.: Interpreting upward methane flux from marine pore water
919 profiles, In: Fire in the Ice, NETL Methane Hydrate Newsletter 9 (1), 7-10, 2009.
920 D'Hondt, S., Rutherford, S., and Spivack, A. J.: Metabolic activity of subsurface life in deep-sea
921 sediments, Science, 295, 2067–2070, 2002.
922 Dmitrenko, I. A., Polyakov, I. V., Kirillov, S. A., Timokhov, L. A., Frolov, I. E., Sokolov, V. T.,
923 Simmons, H. L., Ivanov, V. V., and Walsh, D.: Toward a warmer Arctic Ocean:

spreading of the early 21st century Atlantic Water warm anomaly along the Eurasian Basin margins, J. Geophys. Res-Oceans 113, 1-13, 2008.

Dmitrenko, I. A., Bauch, D., Kirillov, S. A., Koldunov, N., Minnett, P. J., Ivanov, V. V., Hölemann, J. A., and Timokhov, L. A.: Barents Sea upstream events impact the properties of Atlantic water inflow into the Arctic Ocean: Evidence from 2005 to 2006 downstream observations, Deep-Sea Research I, 56, 513–527, 2009.

Donohue, C. M., Snyder, G. T., and Dickens, G. R.: Data report: major cation concentrations of interstitial waters collected from deep sediments of Eastern Equatorial Pacific and Peru Margin (ODP Leg 201), Proceedings of ODP, Scientific Results, 201, Ocean Drilling Program, College Station, TX, 2006.

Dymond, J., Suess, E., and Lyle, M.: Barium in deep-sea sediment: A geochemical proxy for paleoproductivity, Paleoceanography 7, 163–181, 1992.

Elliott, S., Maltrud, M., Reagan, M., Moridis, G., and Cameron-Smith P.: Marine methane cycle simulations for the period of early global warming, J. Geophys. Res-Biogeo., 116, 1-13, 2011.

Engen, Ø., Faleide, J. I., and Dyreng, T. K.: Opening of the Fram Strait gateway: A review of plate tectonic constraints: Tectonophysics, 450, 1-69, 2008.

Expedition 346 Scientists: Asian Monsoon: onset and evolution of millennial-scale variability of Asian monsoon and its possible relation with Himalaya and Tibetan Plateau uplift, IODP Preliminary Report, 346, 2014.

Eiken, O. and Hinz, K.: Contourites in the Fram Strait, Sediment Geol., 82, 15–32, 1993.

945 Ferré, B., Mienert, J., and Feseker, T.: Ocean temperature variability for the past 60 years on the
946 Norwegian-Svalbard margin influences gas hydrate stability on human time scales, J.
947 Geophys. Res., 117, 1-14, 2012.
948 Flood, R. D., Piper, D. J. W., Klaus, A., and Scientific Research Party: Proceedings of the Ocean
949 Drilling Program, Initial Reports, 155: College Station, TX (Ocean Drilling Program),
950 1995.
951 Froelich, P., Klinkhammer, G. P., Bender, M. A. A., Luedtke, N. A., Heath, G. R., Cullen, D.,
952 Dauphin, P., Hammond, D., Hartman, B., and Maynard, V.: Early oxidation of organic
953 matter in pelagic sediments of the eastern equatorial Atlantic: suboxic diagenesis,
954 Geochim. Cosmochim. Ac., 43, 1075-1090, 1979.
955 Gao, H., Schreiber, F., Collins, G., Jensen, M. M., Kostka, J. E., Lavik, G., de Beer, D., Zhou, H.
956 Y., and Kuypers, M. M.: Aerobic denitrification in permeable Wadden Sea sediments,
957 The ISME J., 4, 417-426, 2010.
958 Geprägs, P., Torres, M. E., Mau, S., Kasten, S., Römer, M., and Bohrmann, G.: Carbon cycling
959 fed by methane seepage at the shallow Cumberland Bay, South Georgia, sub-Antarctic,
960 Geochem. Geophy. Geosy., 17, 1401-1418, 2016.
961 Gieskes, J. M. and Rogers, W. C.: Alkalinity determination in interstitial waters of marine
962 sediments, J. Sediment. Res., 43(1), 272-277, 1973.
963 Gieskes, J. M., Gamo, T., and Brumsack, H.: Chemical methods for interstitial water analysis
964 aboard JOIDES Resolution, 1991.
965 Gingele, F. and Dahmke, A.: Discrete barite particles and barium as tracers of paleoproductivity
966 in South Atlantic sediments, Paleoceanography, 9, 151–168, 1994.

967 Giustiniani, M., Tinivella, U., Jakobosson, M., and Rebesco, M.: Arctic Ocean gas hydrate
968 stability in a changing climate, J. Geol. Res., 1-10, 2013.
969 Goldhaber, M.: Kinetic Models of Sulfur Diagenesis in Recent Marine Sediments, In
970 Transactions-AGU, 55, 696-697, 1974.
971 Grantz, A., Boucher, G., and Whitney, O. T.: Possible solid gas hydrate and natural gas deposits
972 beneath the continental slope of the Beaufort Sea, U.S. Geological Survey Circulation
973 Number 733, 1976.
974 Grantz, A., Mann, D. M., and May, S. D.: Tracklines of multichannel seismic-reflection data
975 collected by the U.S. Geological Survey in the Beaufort and Chukchi Seas in 1977 for
976 which profiles and stack tapes are available, U.S. Geological Survey Open-File Report
977 1982, 82-735, 1982.
978 Greinert, J., Bohrmann, G., and Suess, E.: Gas hydrate-associated carbonates and methane-
979 venting at Hydrate Ridge: classification, distribution, and origin of authigenic lithologies,
980 Natural gas hydrates: Occurrence, distribution, and detection, 99-113, 2001.
981 Gualtieri, L., Vartanyan, S., Brigham-Grette, J., and Anderson, P. M.: Evidence for an ice-free
982 Wrangel Island, Northeast Siberia during the Last Glacial Maximum, Boreas 34, 264–
983 273, 2005.
984 Haacke, R. R., Westbrook, G. K., and Riley, M.: Controls on the formation and stability of gas
985 hydrate-related bottom-simulating reflectors (BSRs): a case study from the west Svalbard
986 continental slope, J. Geophys. Res., 113, 1-17, 2008.
987 Hamdan, L. J., Gillevet, P. M., Pohlman, J. W., Sikaroodi, M., Greinert, J., and Coffin, R.B.:
988 Diversity and biogeochemical structuring of bacterial communities across the Porangahau
989 ridge accretionary prism, New Zealand, FEMS Microbiol. Ecol., 77, 518-532, 2011.

990 Haraldsson, C., Anderson, L. G., Hassellöv, M., Hulth, S., and Olsson, K.: Rapid, high-precision
991 potentiometric titration of alkalinity in ocean and sediment pore waters, Deep Sea
992 Research Part I: Oceanographic Research Papers, 44, 2031-2044, 1997.
993 Hart, P. E., Pohlman, J. W., Lorenson, T. D., and Edwards, B. D.: Beaufort Sea Deep-water gas
994 hydrate recovery from a seafloor mound in a region of widespread BSR occurence, in
995 Proceedings of the 7th International Conference on Gas Hydrates (ICGH 2011),
996 Edinburgh, Scotland, 2011.
997 Hensen, C., Zabel, M., Pfiefer, K., Schwenk, T., Kasten, S., Riedinger, N., Schulz, H. D.,
998 Boetius, A.: Control of sulfate porewater profiles by sedimentary events and the
999 significance of anaerobic oxidation of methane for the burial of sulfur in marine
1000 sediments, Geochimica Cosmochimica Acta 67, 2631-2647, 2003.
1001 Holbrook, W. S., Hoskins, H., Wood, W. T., Stephen, R. A., and Lizarralde, D.: Methane hydrate
1002 and free gas on the Blake ridge from vertical seismic profiling, Science, 273, 1840–1843,
1003 1996.
1004 Holmes, R. M., McClelland, J. W., Peterson, B. J., Shiklomanov, I. A., Shiklomanov, A. I.,
1005 Zhulidov, A. V., Gordeev, V. V., and Bobrovitskaya, N. N.: A circumpolar perspective
1006 on fluvial sediment flux to the Arctic Ocean, Global Biogeochem. Cy., 16, 1-14, 2002.
1007 Holler, T., Wegener, G., Knittel, K., Boetius, A., Brunner, B., Kuypers, M. M., and Widdel, F.:
1008 Substantial 13C/12C and D/H fractionation during anaerobic oxidation of methane by
1009 marine consortia enriched in vitro, Environ. Microbiol. Rep., 1, 370-376, 2009.
1010 Hovland, M. and Svensen, H.: Submarine pingoes: Indicators of shallow gas hydrates in a
1011 pockmark at Nyegga, Norwegian Sea, Mar. Geol., 228, 15–23, 2006.

1012 Hu, X., Cai, W. -J, Wang, Y., Luo, S., and Guo X.: Pore-water geochemistry of two contrasting
1013 brine-charged seep stations in the northern Gulf of Mexico continental slope, Mar.
1014 Geochem., 118, 99–107, 2010.
1015 Hu, Y., Feng, D., Liang, Q., Xia, Z., Chen, L., and Chen, D.: Impact of anaerobic oxidation of
1016 methane on the geochemical cycle of redox-sensitive elements at cold-seep stations of the
1017 northern South China Sea. Deep Sea Research Part II: Topical Studies in Oceanography,
1018 2015.
1019 Hustoft, S., Bünz, S., Mienert, J., and Chand, S.: Gas hydrate reservoir and active methane-
1020 venting province in sediments on <20Ma young oceanic crust in the Fram Strait, offshore
1021 NW-Svalbard, Earth Planet. Sc. Lett., 284, 12-24, 2009.
1022 Hyndman, R. D. and Dallimore, S. R.: Natural gas hydrates studies, Canada Recorder, 26, 11–20,
1023 2001.
1024 Jakobsson, M.: Hypsometry and volume of the Arctic Ocean and its constituent seas:
1025 Geochemistry, Geophysics, Geosystems, 3, 5, 1-18, 2002.
1026 Jakobsson, M., Grantz, A., Kristoffersen, Y., and Macnab, R.: Physiographic provinces of the
1027 Arctic Ocean seafloor, GSA Bull., 115, 1443-1455, 2003.
1028 Jakobsson, M., Backman, J., Rudels, B., Nycander, J., Frank, M., Mayer, L., Jokat, W.,
1029 Sangiorgi, F., O'Regan, M., Brinkhuis, H., King, J., and Moran, K.: The early Miocene
1030 Onset of a Ventilated Circulation Regime in the Arctic Ocean: Nature, 447, 21, 986-990,
1031 2007.
1032 Jakobsson, M., Polyak, L., Edwards, M., Kleman, J., and Coakley, B.: Glacial geomorphology of
1033 the Central Arctic Ocean: the Chukchi Borderland and the Lomonosov Ridge, Earth Surf.
1034 Proc. Land., 33, 526-545, 2008.

1035 Jakobsson, M., Andreassen, K., Bjarnadóttir, L. R., Dove, D., Dowdeswell, J. A., England, J. H.,
1036 Funder, S., Hogan, K., Ingólfsson, Ó., Jennings, A., Krog-Larsen, N., Kirchner, N.,
1037 Landvik, J. Y., Mayer, L., Möller, P., Niessen, F., Nilsson, J., O'Regan, M., Polyak, L.,
1038 Nørgaard-Pedersen, N., and Stein, R.: Arctic Ocean glacial history, Quaternary Sci. Rev.,
1039 92, 40-67, 2014.
1040 Jakobsson, M., Nilsson, J., Anderson, L., Backman, J., Björk, G., Cronin, T.M., Kirchner, N.,
1041 Koshurnikov, A., Mayer, L., Noormets, R. and O'Regan, M.: Evidence for an ice shelf
1042 covering the central Arctic Ocean during the penultimate glaciation. Nature
1043 communications, 7, 2016.
1044 Jørgensen, B. B., Bang, M., and Blackburn, T. H.: Anaerobic mineralization in marine sediments
1045 from the Baltic Sea-North Sea transition, Mar. Ecol. Progress Series, 59, 39-54, 1990.
1046 Jørgensen, B. B., Weber, A. and Zopfi, J.: Sulfate reduction and anaerobic methane oxidation in
1047 Black Sea sediments. Deep Sea Research Part I: Oceanographic Research Papers, 48 (9),
1048 2097-2120, 2001.
1049 Jørgensen, B. B., Böttcher, M. E., Lüschen, H., Neretin, L. N., and Volkov, I. I.: Anaerobic
1050 methane oxidation and the deep H2S sink generate isotopically heavy sulfides in Black
1051 Sea sediments, Geochim. Cosmochim. Ac., 68, 2095–2118, 2004.
1052 Jørgensen, B. B. and Parkes, R. J.: Role of sulfate reduction and methane production by organic
1053 carbon degradation in eutrophic fjord sediments (Limfjorden, Denmark), Limnol.
1054 Oceanogr, 55, 1338-1352, 2010.
1055 Jokat, W.: The expedition of the Research Vessel" Polarstern" to the Arctic in 2009 (ARK-
1056 XXIV/3). Berichte zur Polar-und Meeresforschung (Reports on Polar and Marine
1057 Research), 615, 2010.

1058 Jokat, W. and Ickrath, M.: Structure of ridges and basins off East Siberia along 81° N, Arctic
1059 Ocean, Mar. Petrol. Geol., 64, 222-232, 2015.
1060 Joye, S. B., Boetius, A., Orcutt, B. N., Montoya, J. P., Schulz, H. N., Erickson, M. J. and Lugo,
1061 S.K.: The anaerobic oxidation of methane and sulfate reduction in sediments from Gulf
1062 of Mexico cold seeps. Chemical Geology, 205 (3), 219-238, 2004.
1063 Jenkyns, H. C., Forster, A., Schouten, S., and Sinninghe Damsté, J. S.: High temperatures in the
1064 Late Cretaceous Arctic Ocean, Nature, 432, 888–892, 2004.
1065 Judge, A. S.: Natural gas hydrates in Canada, In: M.H. French (Editor), Proceedings of the
1066 Fourth Canadian Permafrost Conference 1981, Roger J.E. Brown Memorial Volume,
1067 National Research Council of Canada, Ottawa, Ont., 320-328, 1982.
1068 Kastner, M., Claypool, G., and Robertson, G.: Geochemical constraints on the origin of the pore
1069 fluids and gas hydrate distribution at Atwater Valley and Keathley Canyon, northern Gulf
1070 of Mexico, Mar. Petr. Geol., 25, 860–872, 2008a.
1071 Kastner, M., Torres, M., Solomon, E., and Spivack, A. J.: Marine pore fluid profiles of dissolved
1072 sulfate; do they reflect in situ methane fluxes?, In: Fire in the Ice, NETL Methane
1073 Hydrate Newsletter, Summer, 2008b.
1074 Keigwin, L. D., Rio, D., Acton, G. D., and Shipboard Scientific Party: Proceedings of the Ocean
1075 Drilling Program, Initial Reports, 172: College Station, TX (Ocean Drilling Program),
1076 1998.
1077 Kimura, G., Silver, E. A., Blum, P., Shipboard Scientific Party: Proceedings of the Ocean
1078 Drilling Program, Initial Reports, Vol. 170, 1997.
1079 Klauda, J. B. and Sandler, S. I.: Global distribution of methane hydrate in ocean sediment,
1080 Energy Fuel, 19, 469–78, 2005.

1081 Klump, J. V. and Martens, C. S.: Biogeochemical cycling in an organic rich coastal marine
1082 basin—II. Nutrient sediment-water exchange processes, Geochim. Cosmochim. Ac., 45,
1083 101-121, 1981.
1084 Kvenvolden, K. A., and Grantz, A.: Gas hydrates in the Arctic Ocean region, in The Arctic
1085 Ocean Region, Geology of North America, Geol. Soc. of Am., Boulder, Colo., 539-549,
1086 1990.
1087 Kvenvolden, K. A.: Gas hydrates: Geological perspective and global change, Rev. Geophys., 31,
1088 173–187, 1993.
1089 Kvenvolden, K. A. and Lorenson, T. D.: The global occurrence of natural gas hydrate. In: Paull,
1090 C. K., Dillon, W. P. (Eds.), Natural Gas Hydrates: Occurrence, Distribution, and
1091 Detection, AGU Geophy. Monograph Ser., 124, 3–18, 2001.
1092 Laberg, J. S. and Andreassen, K.: Gas hydrate and free gas indications within the Cenozoic
1093 succession of the Bojornya Basin, western Barents Sea, Mar. Petrol. Geol., 13, 921-940,
1094 1996.
1095 Laberg, J. S., Andreassen, K., and Knutsen, S. M.: Inferred gas hydrate on the Barents Sea shelf
1096 a model for its formation and a volume estimate, Geo-Mar. Lett., 18, 26–33, 1998.
1097 Lerman, A.: Migrational processes and chemical reactions in Sulfate profiles and barium fronts
1098 in sediment 539 interstitial waters, In The Sea, Volume VI (ed. E. D. Goldberg), Wiley,
1099 New York, 695-738, 1977.
1100 Li, Y-H. and Gregory, S.: Diffusion of ions in sea sediments. Geochim. Cosmochim. Ac., 38,
1101 703-714, 1974.

1102 Lin, S., Hsieh, W. C., Lim, Y. C., Yang, T. F., Liu, C. S., and Wang, Y.: Methane migration and
1103 its influence on sulfate reduction in the Good Weather Ridge region, South China Sea
1104 continental margin sediments, Terr. Atmos. Ocean. Sci., 17, 883-902, 2006.
1105 Lorenson, T. D. and Kvenvolden, K. A.: Methane in coastal seawater, sea ice, and bottom
1106 sediments, Beaufort Sea, Alaska, USGS Open-File Report 95–70, 1995.
1107 Løvø, V., Elverhøi, A., Antonsen, P., Solheim, A., Butenko, G., Gregersen, O., and Liestøl O.:
1108 Submarine permafrost and gas hydrates in the northern Barents Sea, Norsk Polarinstitutt
1109 Rapportserie, 56, 1-171, 1990.
1110 Luff, R. and Wallmann, K.: Fluid flow, methane fluxes, carbonate precipitation and
1111 biogeochemical turnover in gas hydrate-bearing sediments at hydrate ridge, Cascadia
1112 margin: numerical modeling and mass balances, Geochim. Cosmochim. Ac., 67, 3403–
1113 3421, 2003.
1114 Luo, M., Chen, L., Wang, S., Yan, W., Wang, H., and Chen, D.: Pockmark activity inferred from
1115 pore water geochemistry in shallow sediments of the pockmark field in southwestern
1116 Xisha Uplift, northwestern South China Sea, Mar. Pet. Geol., 2013, 48, 247–259, 2013.
1117 Lyle, M., Koizumi, I., Richter, C., and Shipboard Scientific Party: Proceedings of the Ocean
1118 Drilling Program, Initial Reports, Vol. 167, 1997.
1119 MacKay, M. E., Jarrard, R. D., Westbrook, G. K., Hyndman, R. D., and Shipboard Scientific
1120 Party: Origin of bottom-simulating reflectors: geophysical evidence from the Cascadia
1121 accretionary prism, Geol., 22, 459–462, 1994.
1122 Majorowicz, J. A. and Osadetz, K. G.: Gas hydrate distribution and volume in Canada. AAPG
1123 bulletin, 85 (7), 1211-1230, 2001.

1124 Makogon, Y. F.: Natural gas hydrates–A promising source of energy, J. Nat. Gas Sc. Eng., 2, 49-
1125 59, 2010.
1126 Malinverno, A. and Pohlman, J. W.: Modeling sulfate reduction in methane hydrate-bearing
1127 continental margin sediments: does a sulfate-methane transition require anaerobic
1128 oxidation of methane, Geochem. Geophy. Geosy., 12, 1-18, 2011.
1129 März, C., Stratmann, A., Matthiessen, J., Meinhardt, A. K., Eckert, S., Schnetger, B., Vogt, C.,
1130 Stein, R. and Brumsack, H. J.: Manganese-rich brown layers in Arctic Ocean sediments:
1131 composition, formation mechanisms, and diagenetic overprint. Geochimica et
1132 Cosmochimica Acta, 75 (23), 7668-7687, 2011.
1133 Max, M. D. and Lowrie, A.: Natural gas hydrates: Arctic and Nordic Sea potential. Arctic
1134 geology and petroleum potential, proceedings of the Norwegian Petroleum Society
1135 conference, 15-17 August 1990, Tromsø, Norway. No. 2. Elsevier Science Ltd., 1993.
1136 Max, M. D. and Johnson, A. H.: Natural Gas Hydrate (NGH) Arctic Ocean potential prospects
1137 and resource base, OTC Arctic Technology Conference, 27-53, 2012.
1138 McGuire, A. D., Anderson, L. G., Christensen, T. R., Dallimore, S., Guo, L. D., Hayes, D. J.,
1139 Heimann, M., Lorenson, D. D., MacDonald, R. W., and Roulet, N.: Sensitivity of the
1140 carbon cycle in the Arctic to climate change, Ecol. Monogr., 79, 523–555, 2009.
1141 Miles, P. R.: Potential distribution of methane hydrate beneath the European continental margins,
1142 Geophys. Res. Lett., 22, 3179-3182, 1995.
1143 Miller, C., Vasconcelos, K.L., Little, D.N. and Bhasin, A.: Investigating aspects of aggregate
1144 properties that influence asphalt mixtures performance. Research Report for DTFH61-06-
1145 C-00021, Texas A&M University at College Station and The University of Texas at
1146 Austin, Texas, 2011.

1147 Miller, C., Little, D., Bhasin, A., Gardner, N. and Herbert, B., 2012. Surface energy
1148 characteristics and impact of natural minerals on aggregate-bitumen bond strengths and
1149 asphalt mixture durability. Transportation Research Record: Journal of the Transportation
1150 Research Board, (2267), 45-55, 2012.
1151 Miller, M. D., Adkins, J. F., and Hodell, D. A.: Rhizon sampler alteration of deep ocean
1152 sediment interstitial water samples, as indicated by chloride concentration and oxygen
1153 and hydrogen isotopes, Geochem. Geophy. Geosy., 15, 2401-2413, 2014.
1154 Moore, G. F., Taira, A., and Klaus, A., and Shipboard Scientific Party: Proceedings of the Ocean
1155 Drilling Program, Initial Reports Volume 190, 2001.
1156 Moran, K., Backman, J., Brinkhuis, H., Clemens, S. C., Cronin, T., Dickens, G. R., Eynaud, F.,
1157 Gattacceca, J., Jakobsson, M., Jordan, R.W., and Kaminski, M.: The Cenozoic
1158 palaeoenvironment of the arctic ocean, Nature, 441, 601-605, 2006.
1159 Mountain, G. S., Miller, K. G., Blum, P., and Shipboard Scientific Party: Proc. ODP, Initial
1160 Reports, 150: College Station, TX (Ocean Drilling Program), 1994.
1161 Murray, R. W., Miller, D. J., and Kryc, K. A.: Analysis of major and trace elements in rocks,
1162 sediments, and interstitial waters by inductively coupled plasma–atomic emission
1163 spectrometry (ICP-AES), ODP Technical Note 29, 2000.
1164 Naidu, A. S., Cooper, L. W., Finney, B. P., Macdonald, R. W., Alexander, C., and Semiletov, I.
1165 P.: Organic carbon isotope ratios (δ13C) of Arctic Amerasian continental shelf sediments,
1166 Int. J. Earth Sci., 89, 522–532, 2000.
1167 Niessen, F., Hong, J. K., Hegewald, A., Matthiessen, J., Stein, R., Kim, H., Kim, S., Jensen, L.,
1168 Jokat, W., Nam, S.-I., and Kang, S.-H.: Repeated Pleistocene glaciation of the East
1169 Siberian Continental Margin, Nat. Geosci., 6, 842-846, 2013.

Niewohner, C., Hensen, C., Kasten, S., Zabel, M., and Schulz, H. D.: Deep sulfate reduction completely mediated by anaerobic methane oxidation in sediments of the upwelling area off Namibia, Geochim. Cosmochim. Ac., 62, 455–464, 1998.

Nöthen, K. and Kasten, S.: Reconstructing changes in seep activity by means of pore water and solid phase Sr/Ca and Mg/Ca ratios in pockmark sediments of the Northern Congo Fan, Mar. Geol., 287, 1-13, 2011.

O'Regan, M., Williams, C. J., Frey, K. E., Jakobsson, M.: A synthesis of the long-term paleoclimatic evolution of the Arctic. Oceanography 24(3), 66–80, 2011.

O'Regan, M., Preto, P., Stranne, C., Jakobsson, M., and Koshurnikov, A.: Surface heat flow measurements from the East Siberian continental slope and southern Lomonosov Ridge, Arctic Ocean, Geochem. Geophy. Geosy., 17, 1-15, 2016.

Ostanin, I., Anka, Z., di Primio, R. and Bernal, A.: Hydrocarbon plumbing systems above the Snøhvit gas field: structural control and implications for thermogenic methane leakage in the Hammerfest Basin, SW Barents Sea. Marine and Petroleum Geology, 43, 127-146, 2013.

Party, S. S.: Integrated Ocean Drilling Program Expedition 303 Preliminary Report North Atlantic Climate Ice sheet–ocean atmosphere interactions on millennial timescales during the late Neogene-Quaternary using a paleointensity-assisted chronology for the North Atlantic, 1-51, 2005.

Paull, C. K., Ussler, W. III, and Dillon, W. P.: Is the extent of glaciation limited by marine gas-hydrates?, Geophys. Res. Lett., 18 432–434, 1991.

Paull, C. K., Matsumoto, R., Wallace, P. J., and Shipboard Scientific Party: Proceedings of the IODP, Initial Reports. Volume 164: College Station, TX, USA, 1996.

Paull, C. K, Lorenson, T. D., Borowski, W. S., Ussler, III W., Olsen, K., and Rodriguez, N. M.: Isotopic composition of CH_4, CO_2 species, and sedimentary organic matter within samples from the Blake Ridge: gas source implications, In: Paull C. K., Matsumoto, R, Wallace, P. J., and Dillon, W. P., (Eds) Proceedings of the ODP, Sci. Res., Vol. 164 67–78, (ODP), 2000.

Pecher, I. A., Kukowski, N., Huebscher, C., Greinert, J., and Bialas, J.: The link between bottom-simulating reflections and methane flux into the gas hydrate stability zone - new evidence from Lima Basin, Peru Margin, Earth Planet. Sc. Lett., 185, 343-354, 2001.

Peterson, B. J., Holmes, R. M., McClelland, J. W., Vorosmarty, C. J., Lammers, R. B., Shiklomanov, A. I., Shiklomanov, I. A., and Rahmstorf, S.: Increasing river discharge to the Arctic Ocean, Science, 298, 2171–2173, 2002.

Petersen, C. J., Bünz, S., Hustoft, S., Mienert, J., and Klaeschen, D.: High-resolution P-Cable 3D seismic imaging of gas chimney structures in gas hydrated sediments of an Arctic sediment drift, Mar. Petrol. Geol., 1–14, 2010.

Phrampus, B. J., Hornbach, M. J., Ruppel, C. D., and Hart P. E.: Widespread gas hydrate instability on the upper US Beaufort margin, J. Geophys. Res-Sol. Ea., 119, 8594–8609, 2014.

Piñero, E., Marquardt, M., Hensen, C., Haeckel, M., and Wallmann K.: Estimation of the global inventory of methane hydrates in marine sediments using transfer functions, Biogeosciences 10, 959–975, 2013.

Pohlman, J. W., Riedel, M., Waite, W., Rose, K., and Lapham, L.: Application of Rhizon samplers to obtain high-resolution pore-fluid records during geo-chemical investigations

of gas hydrate systems, Fire in the Ice: Methane Hydrate Newsletter, US Department of Energy/National Energy Technology Laboratory, Fall, 2008.

Posewang, J. and Mienert, J.: High-resolution seismic studies of gas hydrates west of Svalbard, Geo-Mar. Lett., 19, 150–156, 1999.

Prell, W. L., Niitsuma, N., and Shipboard Scientific Party: Proceedings of the Ocean Drilling Program, Initial Reports, 117: College Station, TX (Ocean Drilling Program), 1998.

Rachor, E.: The expedition ARK-XI/1 of RV" Polarstern" in 1995: [ARK XI/1, Bremerhaven-Tromsø-, 07.07. 1995-20.09. 1995]. Berichte zur Polarforschung (Reports on Polar Research), 226, 1995.

Reagan, M. T. and Moridis, G. J.: Dynamic response of oceanic hydrate deposits to ocean temperature change, J. Geophys. Res., 113, 1-21, 2008.

Reagan, M. T. and Moridis, G. J.: Large-scale simulation of methane hydrate dissociation along the West Spitsbergen margin, Geophys. Res. Lett., 36, 1-5, 2009.

Redfield, A. C.: The biological control of chemical factors in the environment, Am. Sci., 46, 221-230, 1958.

Regnier, P., Dale, A. W., Arndt, S., LaRowe, D. E., Mogollón, J., and Van Cappellen, P.: Quantitative analysis of anaerobic oxidation of methane (AOM) in marine sediments: a modeling perspective, Earth-Sci. Rev., 106, 105-130, 2011.

Reeburgh, W. S.: Methane consumption in Cariaco Trench waters and sediments, Earth Planet Sci. Lett., 28, 337–344, 1976.

Riedel, M., Collett, T.S., Malone, M.J., and the Expedition 311 Scientists Proceedings of the Integrated Ocean Drilling Program, Volume 311, 2006.

1237 Riedinger, N., Kasten, S., Gröger, J., Franke, C. and Pfeifer, K.: Active and buried authigenic
1238 barite fronts in sediments from the Eastern Cape Basin, Earth Planet. Sc. Lett., 241, 876-
1239 887, 2006.
1240 Riedinger, N., Formolo, M. J., Lyons, T. W., Henkel, S., Beck, A., and Kasten, S.: An inorganic
1241 geochemical argument for coupled anaerobic oxidation of methane and iron reduction in
1242 marine sediments, Geobiology, 12, 172-181, 2014.
1243 Rudels, B., Muench, R. D., Gunn, J., Schauer, U., and Friedrich, H. J.: Evolution of the Arctic
1244 Ocean boundary current north of the Siberian shelves, Journal of Marine Systems, 25, 1,
1245 77-99, 2000.
1246 Ryan, W. B. F., Carbotte, S. M., Coplan, J. O., O'Hara, S., Melkonian, A., Arko, R., Weissel, R.
1247 A., Ferrini, V., Goodwillie, A., Nitsche, F., Bonczkowski, J., and Zemsky, R.: Global
1248 Multi-Resolution Topography synthesis, Geochem. Geophys. Geosyst., 10, 1-9, 2009.
1249 Schrum, H. S., Murray, R. S., and Gribsholt B.: Comparison of rhizon sampling and whole round
1250 squeezing for marine sediment porewater, Sci. Drill., 13, 47–50, 2012.
1251 Schulz, H. D.: Quantification of early diagenesis: dissolved constituents in marine pore water, In
1252 Mar. Geochem., Springer Berlin Heidelberg, 85-128, 2000.
1253 Seeberg-Elverfeldt, J., Schlüter, M., Feseker, T., and Kölling, M.: Rhizon sampling of pore
1254 waters near the sediment/water interface of aquatic systems, Limnol. Oceanogr. Methods,
1255 3, 361-371, 2005.
1256 Seifert, R. and Michaelis, W.: Organic compounds in sediments and pore waters of Sites 723 and
1257 724, In Prell, W.L., Niitsuma, N., et al., Proc. ODP, Sci. Results, 117: College Station,
1258 TX (ODP), 529–545, 1991.

1259 Serreze, M. C., Walsh, J. E., Chapin, III F. S., Osterkamp, T., Dyurgerov, M., Romanovsky, V.,
1260 Oechel, W. C., Morison, J., Zhang T., and Barry, R. B.: Observational evidence of recent
1261 change in the northern high-latitude environment, Climatic Change, 46, 159–207, 2000.
1262 Semiletov, I., Makshtas, O. A., Akasofu, S.I., and Andreas, E. L.: Atmospheric CO2 balance: the
1263 role of Arctic sea ice, Geophys. Res. Lett., 31, 1-4, 2004.
1264 Shakhova, N, Semiletov, I, Salyuk, A, Yusupov, V, Kosmach, D, and Gustafsson, Ö.: Extensive
1265 Methane venting to the atmosphere from sediments of the East Siberian arctic shelf,
1266 Science, 327, 1246–1250, 2010a.
1267 Shakhova, N., Semiletov, I., Leifer, I., Rekant, P., Salyuk, A., and Kosmach, D.: Geochemical
1268 and geophysical evidence of methane release from the inner East Siberian Shelf, J.
1269 Geophys. Res., 115, 1-14, 2010b.
1270 Sher, A. V., Kuzmina, S. A., Kuznetsova, T. V., and Sulerzhitsky, L. D.: New insights into the
1271 Weichselian environment and climate of the East Siberian Arctic, derived from fossil
1272 insects, plants, and mammals, Quaternary Sci. Rev., 24, 533 – 569, 2005.
1273 Shipboard Scientific Party: Leg 201 summary, In D'Hondt, S.L., Jørgensen, B.B., Miller, D.J., et
1274 al., Proc. ODP, Init. Repts., 201: College Station TX (Ocean Drilling Program), 1–81,
1275 2003.
1276 Sluijs, A., Schouten, S., Pagani, M., Woltering, M., Brinkhuis, H., Damsté, J.S.S., Dickens, G.R.,
1277 Huber, M., Reichart, G.J., Stein, R. and Matthiessen, J.,: Subtropical Arctic Ocean
1278 temperatures during the Palaeocene/Eocene thermal maximum. Nature, 441 (7093), 610-
1279 613, 2006.

1280 Smith, J. P. and Coffin, R. B.: Methane Flux and Authigenic Carbonate in Shallow Sediments
1281 Overlying Methane Hydrate Bearing Strata in Alaminos Canyon, Gulf of Mexico,
1282 Energies, 7, 6118-6141, 2014.
1283 Snyder, G. T., Hiruta, A., Matsumoto, R., Dickens, G. R., Tomaru, H., Takeuchi, R.,
1284 Komatsubara, J., Ishida, Y., and Yu, H.: Porewater profiles and authigenic mineralization
1285 in shallow marine sediments above the methane-charged system on Umitaka Spur, Japan
1286 Sea. Deep-Sea Research II 54, 1216–1239, 2007.
1287 Soloviev, V. A.: Gas-hydrate-prone areas of the ocean and gas-hydrate accumulations, Journal of
1288 the Conference Abstracts, 6, 158, 2002.
1289 Spielhagen, R. F., Werner, K., Sorensen, S. A., Zamelczyk, K., Kandiano, E., Budeus, G.,
1290 Husum, K., Marchitto, T. M., and Hald, M.: Enhanced modern heat transfer to the Arctic
1291 by warm Atlantic water, Science 331, 450-453, 2011.
1292 Stein, R., Boucsein, B., and Meyer, H.: Anoxia and high primary production in the Paleogene
1293 central Arctic Ocean: First detailed records from Lomonosov Ridge, Geophys. Res. Lett.,
1294 33, 1-6, 2006.
1295 Stein, R.: Arctic Ocean sediments: processes, proxies, and paleoenvironment, Developments in
1296 Mar. Geol., 2. Elsevier, Amsterdam. 592, 2008.
1297 Stranne, C., O'Regan, M., Dickens, G. R., Crill, P., Miller, C., Preto, P., and Jakobsson, M.:
1298 Dynamic simulations of potential methane release from East Siberian continental slope
1299 sediments, Geochem. Geophy. Geosy., 17, 872-886, 2016.
1300 Stroeve, J. C., Serreze, M. C., Holland, M. M., Kay, J. E., Malanik, J., and Barrett, A. P.: The
1301 Arctic's rapidly shrinking sea ice cover: a research synthesis, Climatic Change, 110,
1302 1005-1027, 2012.

1303 Suess, E., von Huene, R., and Shipboard Scientific Party: Proceedings of the Ocean Drilling
1304 Program, Initial Reports, 112: College Station, TX (Ocean Drilling Program), 1988.
1305 Takahashi, T. Broecker, V. S., and Langer, S.: Redfield ratio based on chemical data from
1306 isopycnal surfaces, J. Geophys. Res-Oceans, 90, 6907-6924, 1985.
1307 Takahashi, K., Ravelo, A.C., Alvarez Zarikian, C.A., and the Expedition 323 Scientists
1308 Proceedings of the Integrated Ocean Drilling Program, Volume 323, 2011.
1309 Tamaki, K., Pisciotto, K., Allan, J., and Shipboard Scientific Party: Proceedings of the Ocean
1310 Drilling Program, Initial Reports, Vol. 127, 1990.
1311 Thatcher, K. E., Westbrook, G. K., Sarkar, S., and Minshull, T. A.: Methane release from
1312 warming-induced hydrate dissociation in the West Svalbard continental margin: Timing,
1313 rates, and geological controls, J. Geophys. Res-Sol. Ea., 118, 22–38, 2013.
1314 Tian, H., Chen, G., Zhang, C., Melillo, J.M. and Hall, C.A.: Pattern and variation of C: N: P
1315 ratios in China's soils: a synthesis of observational data. Biogeochemistry, 98(1-3),
1316 pp.139-151, 2010.
1317 Timokhov L. A.: Regional characteristics of the Laptev and the East Siberian seas: climate,
1318 topography, ice phases, thermohaline regime, and circulation, In: Russian-German
1319 cooperation in the Siberian Shelf seas: geo-system Laptev Sea, H. Kassens, H. W.
1320 Hubberten, S. Priamikov and R. Stein, editors. Berichte zur Polarforschung, 144, 15-31,
1321 1994.
1322 Torres, M.E., McManus, J., Hammond, D.E., De Angelis, M.A., Heeschen, K.U., Colbert, S.L.,
1323 Tryon, M.D., Brown, K.M. and Suess, E.: Fluid and chemical fluxes in and out of
1324 sediments hosting methane hydrate deposits on Hydrate Ridge, OR, I: Hydrological
1325 provinces. Earth and Planetary Science Letters, 201(3), pp.525-540, 2002.

1326 Torres, M. E., Kastner, M., Wortmann, U. G., Colwell, F., and Kim, J.: Estimates of methane
1327 production rates based on δ13C of the residual DIC in pore fluids from the Cascadia
1328 margin, EOS, 8(52), Fall Meet. Suppl., Abstract GC14A04, 2007.
1329 Torres, M. E. and Kastner M.: Data report: Clues about carbon cycling in methane-bearing
1330 sediments using stable isotopes of the dissolved inorganic carbon, IODP Expedition 311,
1331 Proceedings of the IODP, 311, 2009.
1332 Treude, T., Krause, S., Maltby, J., Dale, A.W., Coffin, R. and Hamdan, L.J.: Sulfate reduction
1333 and methane oxidation activity below the sulfate-methane transition zone in Alaskan
1334 Beaufort Sea continental margin sediments: Implications for deep sulfur cycling.
1335 Geochimica et Cosmochimica Acta, 144, 217-237, 2014.
1336 Troup, B. N., Bricker, O. P., and Bray, J. T.: Oxidation effect on the analysis of iron in the
1337 interstitial water of recent anoxic sediments, Nature 249, 237-239, 1974.
1338 Ussler, W. and Paull, C.K.: Rates of anaerobic oxidation of methane and authigenic carbonate
1339 mineralization in methane-rich deep-sea sediments inferred from models and
1340 geochemical profiles. Earth and Planetary Science Letters, 266(3), 271-287, 2008.
1341 Vanneste, M., Guidard, S., and Mienert, J.: Bottom-simulating reflections and geothermal
1342 gradients across the western Svalbard margin, Terra Nova, 17, 510–516, 2005.
1343 Wallmann, K., Pinero, E., Burwicz, E., Haeckel, M., Hensen, C., Dale, A. W., and Ruepke, L.:
1344 The global inventory of methane hydrate in marine sediments: A theoretical approach,
1345 Energies, 5, 2449–2498, 2012.
1346 Weaver, J. S. and Stewart, J. M.: In-situ hydrates under the Beaufort Sea Shelf, In: M.H. French
1347 (Editor), Proceedings of the Fourth Canadian Permafrost Conference 1981, Roger J. E.
1348 Brown Memorial Volume, Nat. Res. Council Can., Ottawa, Ont., 312-319, 1982.

1349 Wefer, G., Berger, W. H., Richter, C., and Shipboard Scientific Party: Proceedings of the Ocean
1350 Drilling Program, Initial Reports, 175: College Station, TX (Ocean Drilling Program),
1351 1998.
1352 Whiticar, M. J.: Carbon and hydrogen isotope systematics of bacterial formation and oxidation of
1353 methane. Chemical Geology, 161 (1), 291-314, 1999.
1354 Woodgate R. A., Aaagard, K., Muench, R. D., Gunn, J., Björk, G., Rudels, B., Roach, A. T., and
1355 Schauer, U.: The Arctic Ocean boundary current along the Eurasian slope and the
1356 adjacent Lomonosov Ridge: Water mass properties, transports and transformation from
1357 moored instruments, Deep Sea Research, 48, 1757-1792, 2001.
1358 Yamamoto, K. and Dallimore, S.: Aurora-JOGMEC-NRCan Mallik 2006–2008 Gas Hydrate
1359 Research Project progress. In: Fire in the Ice, NETL Methane Hydrate Newsletter,
1360 Summer 2008, 1–5, 2008.
1361 Ye, H., Yang, T., Zhu, G., Jiang, S., and Wu, L.: Pore water geochemistry in shallow sediments
1362 from the northeastern continental slope of the South China Sea, Mar. Petrol. Geol., 75,
1363 68-82, 2016.
1364 Yoshinaga, M. Y., Holler, T., Goldhammer, T., Wegener, G., Pohlman, J. W., Brunner, B.,
1365 Kuypers, M. M., Hinrichs, K. U. and Elvert, M.: Carbon isotope equilibration during
1366 sulphate-limited anaerobic oxidation of methane. Nature Geoscience, 7(3), 190-194,
1367 2014.
1368

Figures

Figure 1.

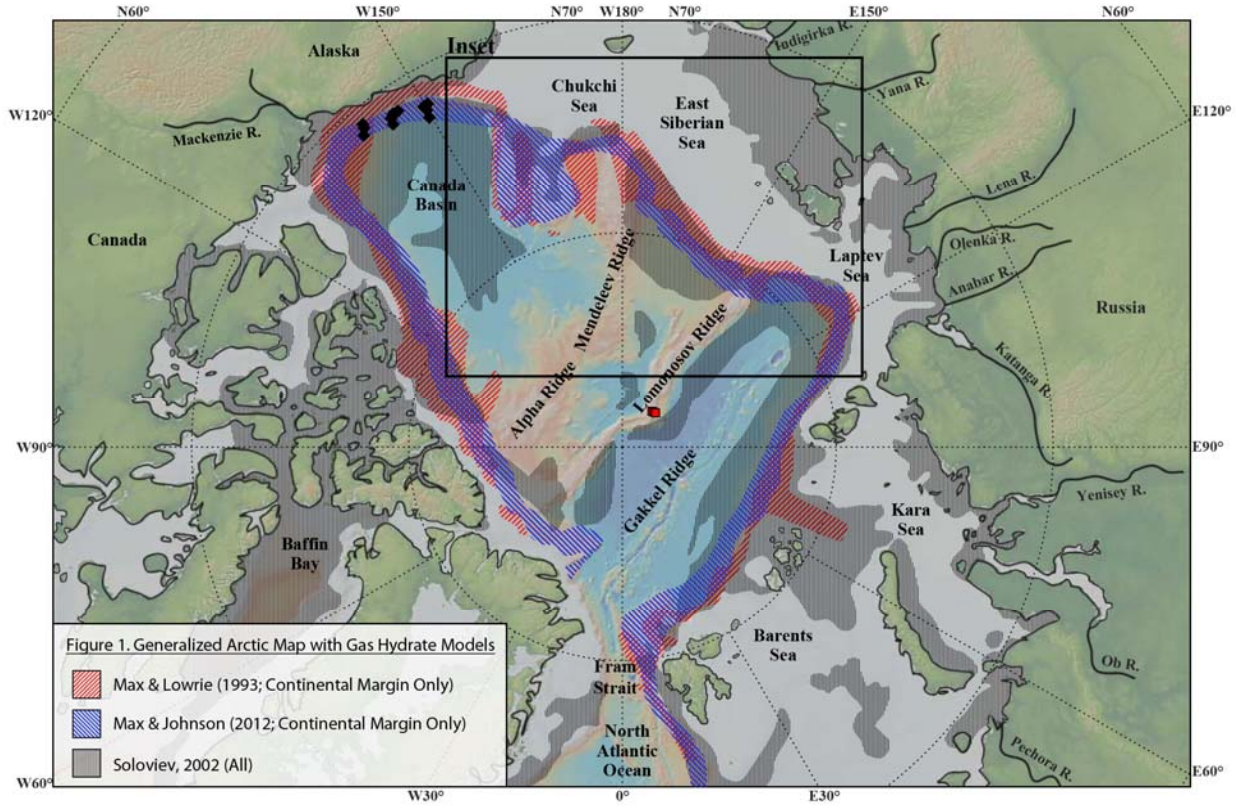

Figure 2.

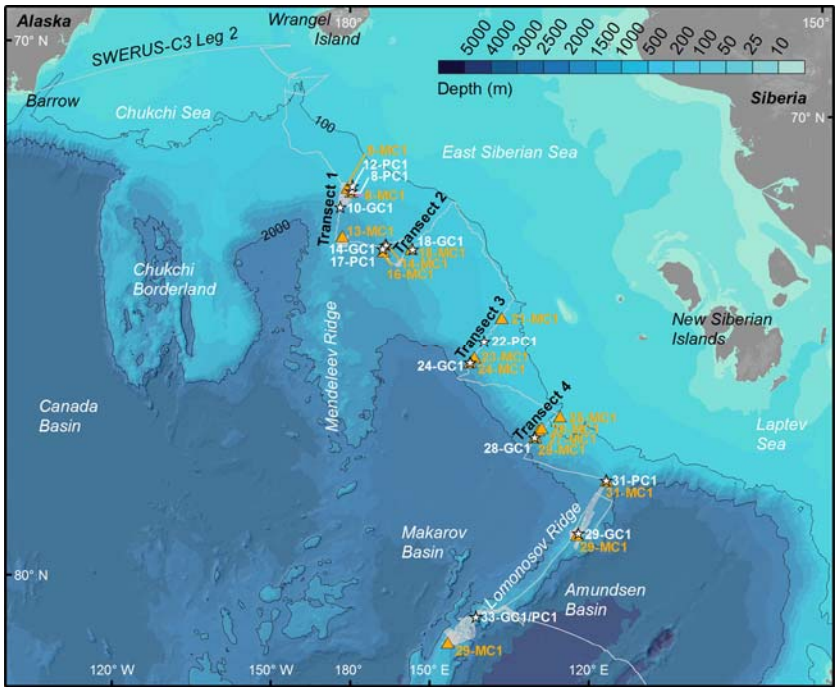
Alaska
70° N
SWERUS-C3 Leg 2
Wrangel Island
180°
150°
Depth (m)
5000
4000
3000
2500
2000
1500
1000
500
200
100
50
25
10
Barrow
Chukchi Sea
Siberia
70° N
East Siberian Sea
100
2000
Transect 1
Transect 2
Transect 3
Transect 4
12-PC1
8-PC1
9-MC1
10-GC1
13-MC1
14-GC1
17-PC1
18-GC1
15-MC1
16-MC1
Chukchi Borderland
Mendeleev Ridge
New Siberian Islands
22-PC1
24-GC1
28-GC1
31-PC1
31-MC1
29-GC1
29-MC1
Canada Basin
Laptev Sea
Makarov Basin
Lomonosov Ridge
Amundsen Basin
33-GC1/PC1
29-MC1
80° N
120° W
150° W
180°
150° E
120° E

1392 **Figure 3.**

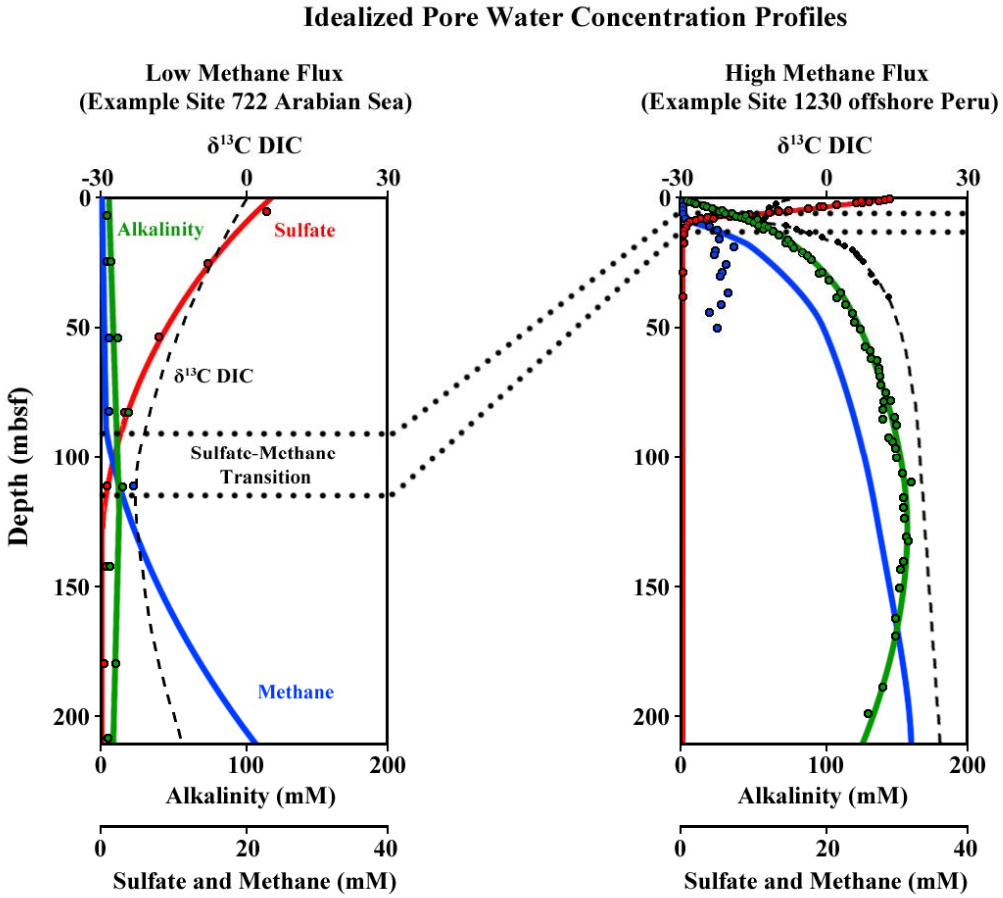

1393

1394 **Figure 4.**

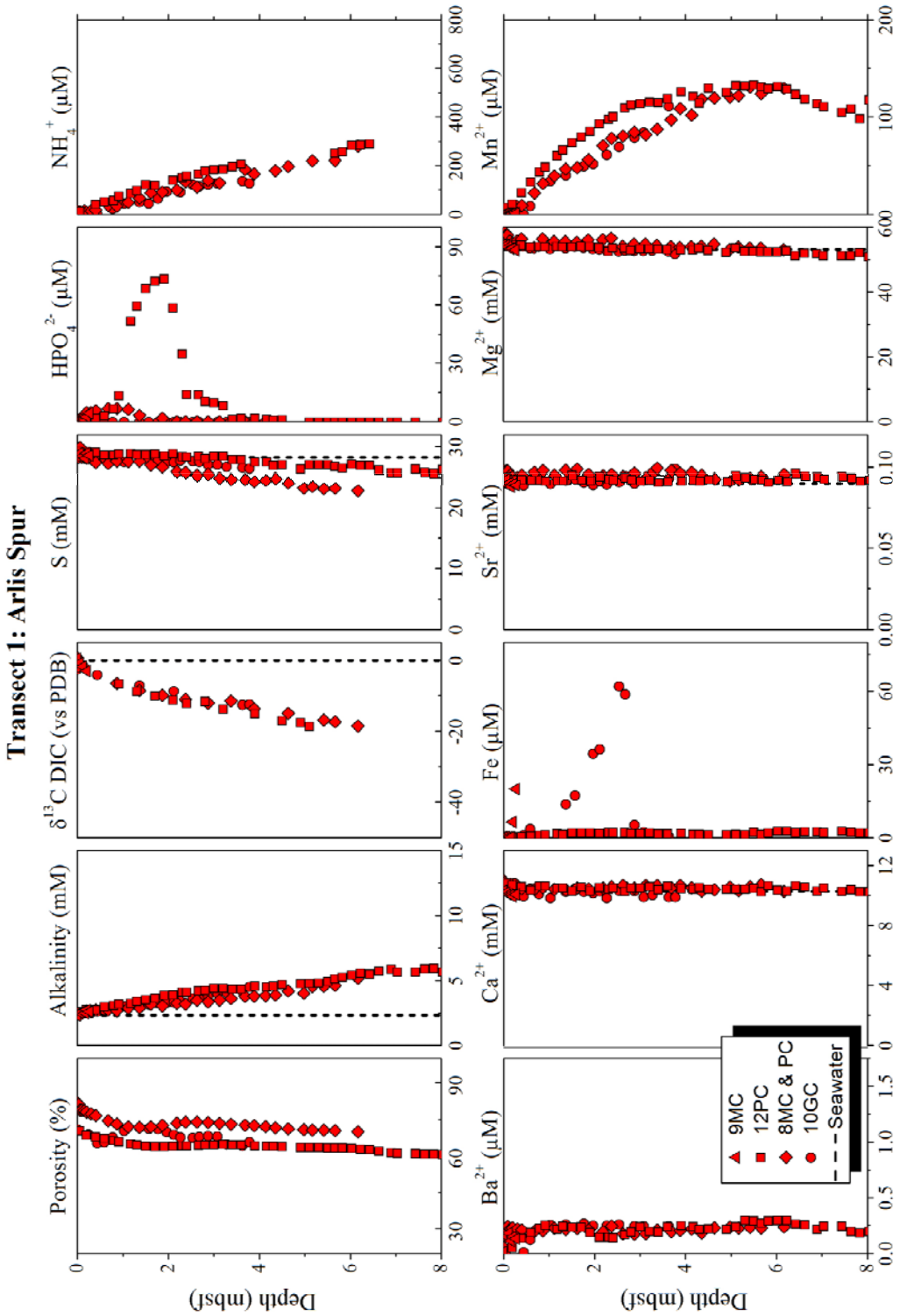

1395

1396

1397 **Figure 5.**

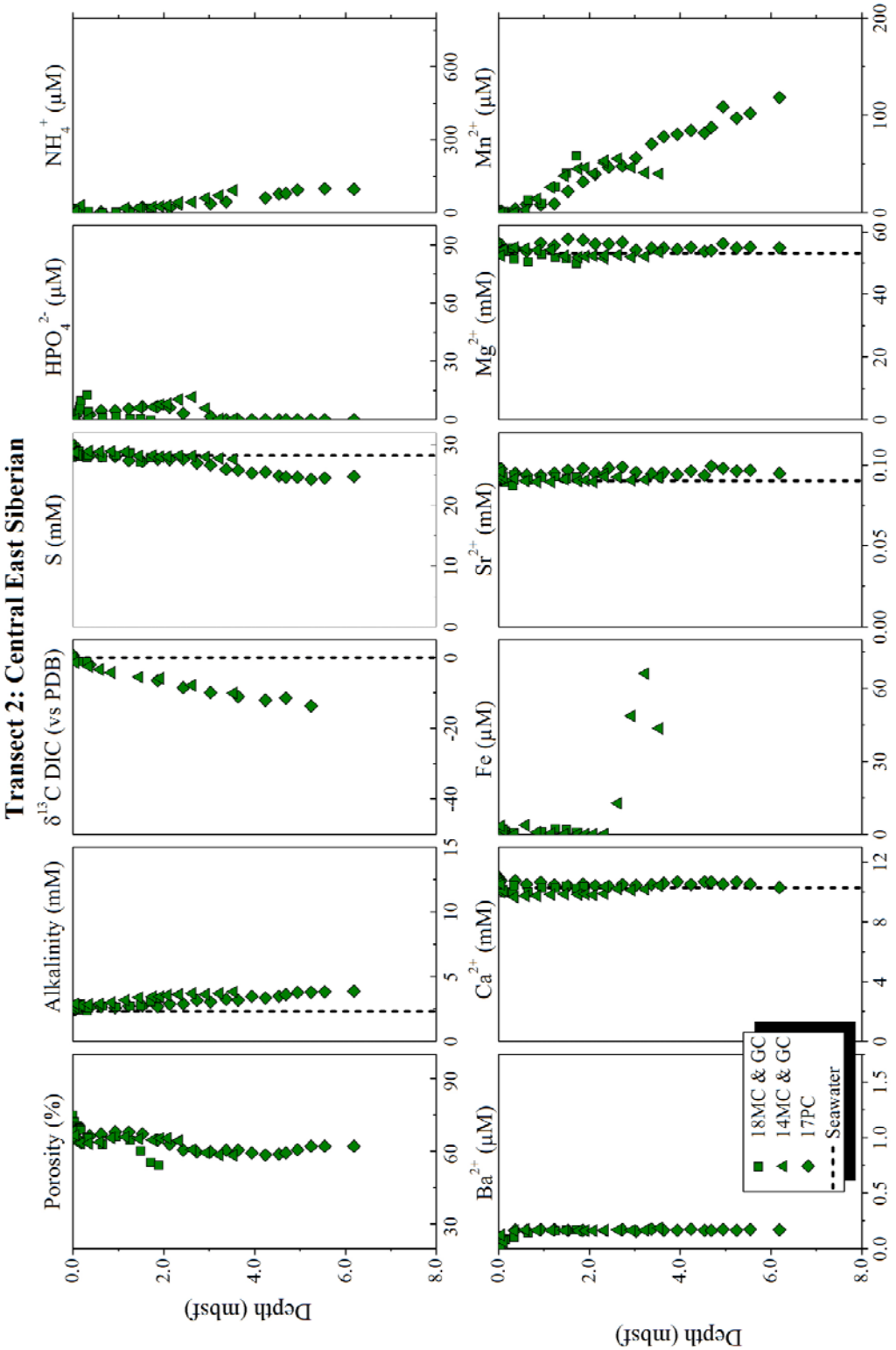

1398

1399

1400 **Figure 6.**

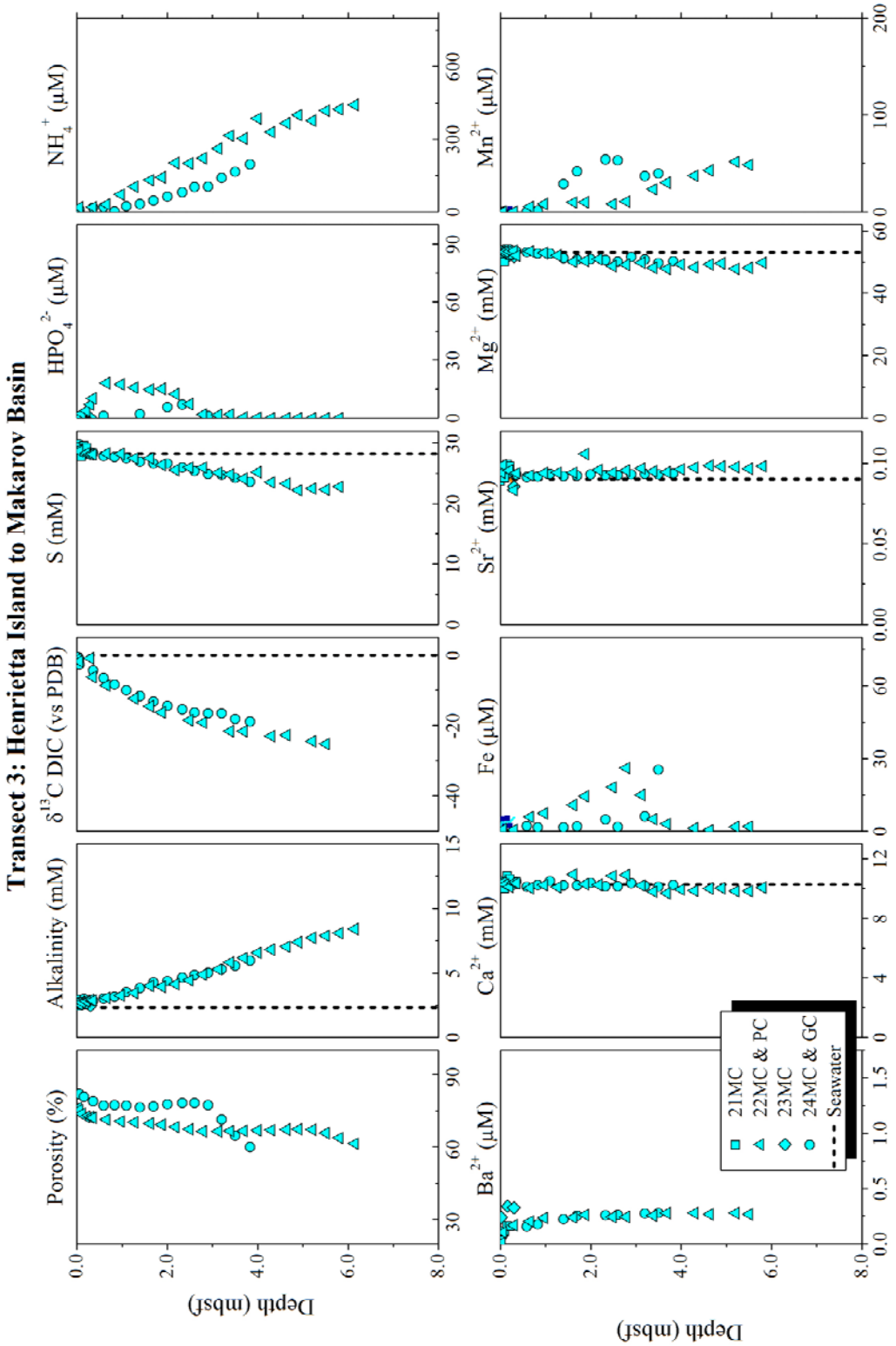

1401

1402

1403 **Figure 7.**

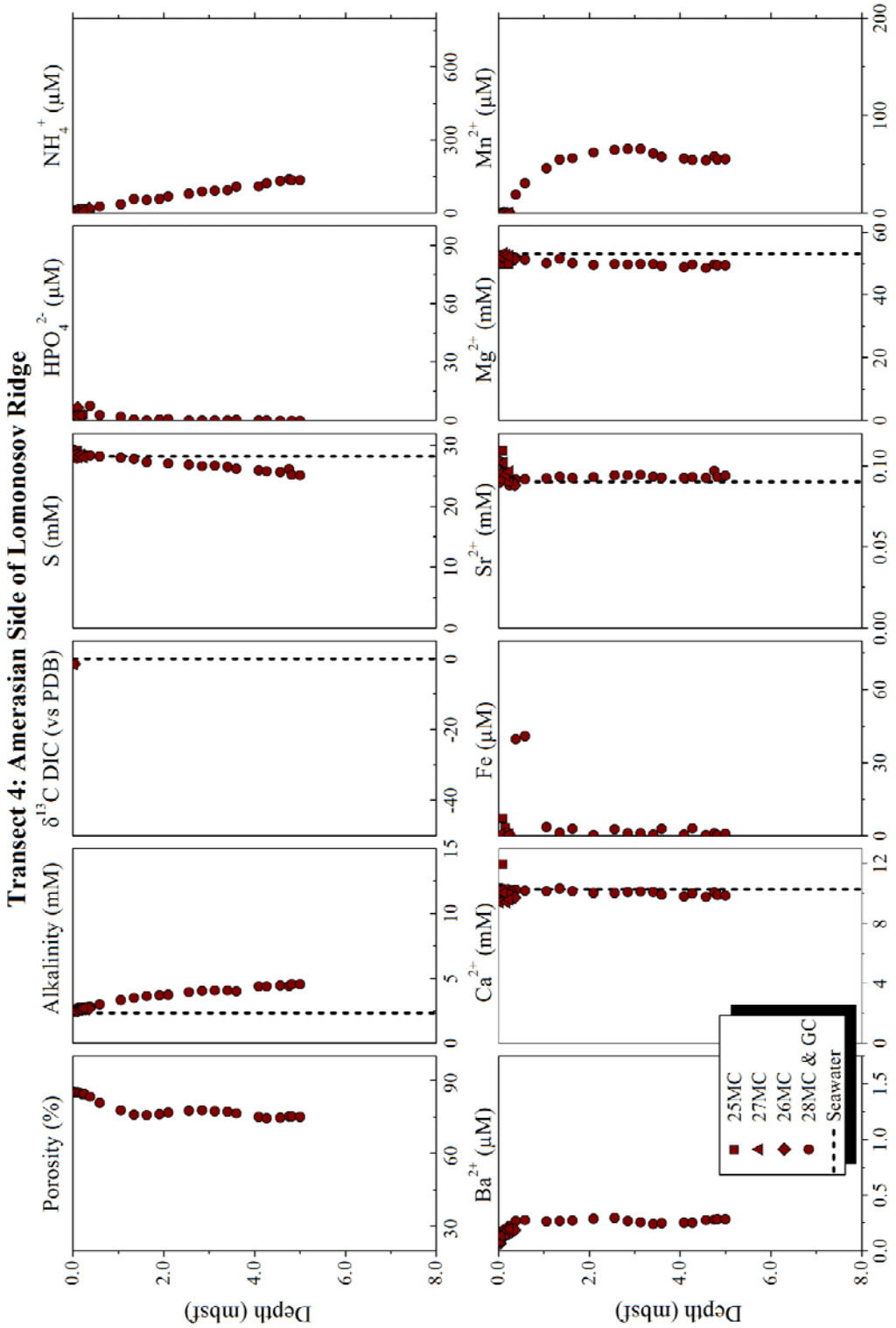

1404

1405

1406 **Figure 8.**

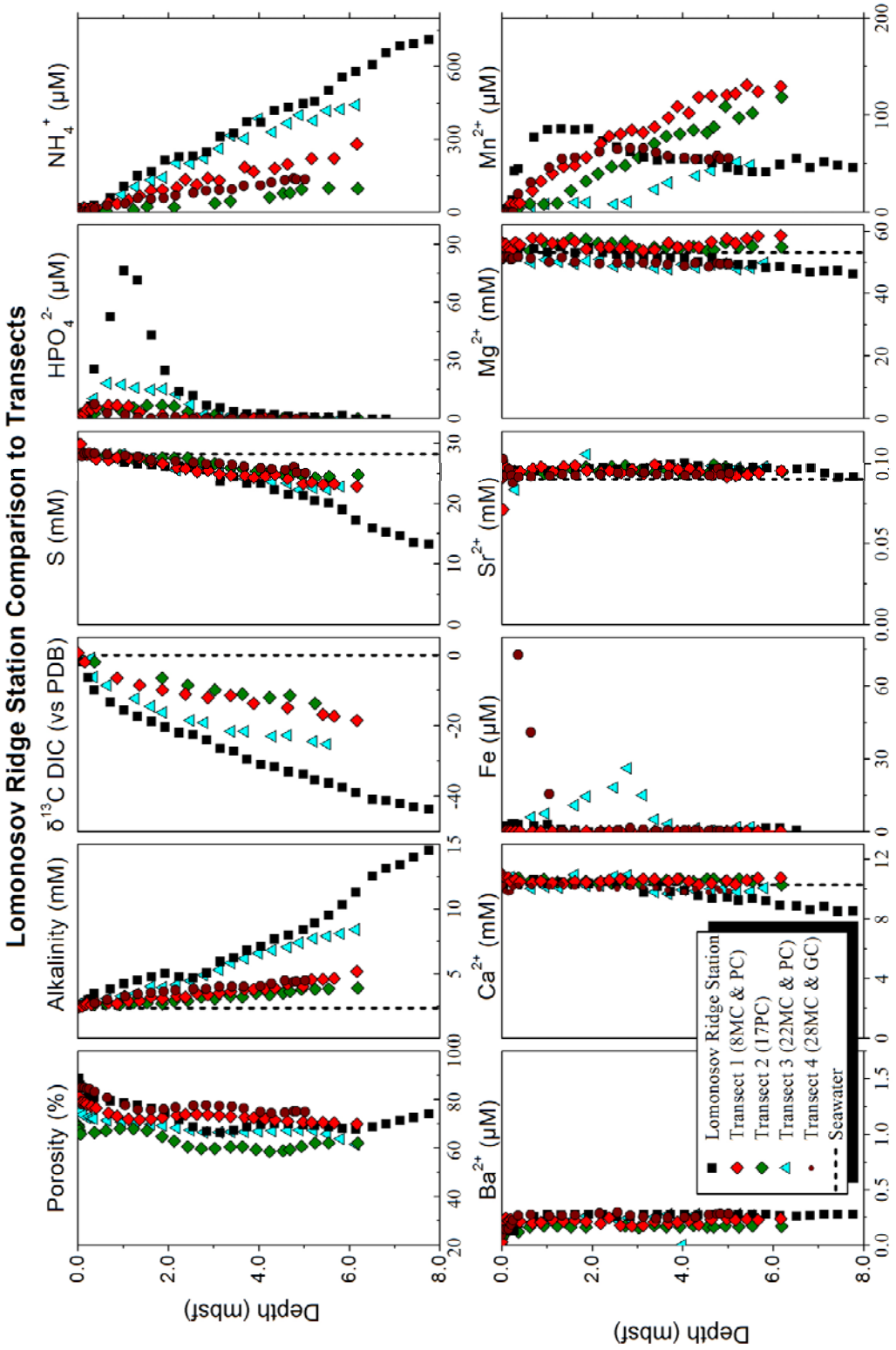

1407

1408

1409 **Figure 9.**

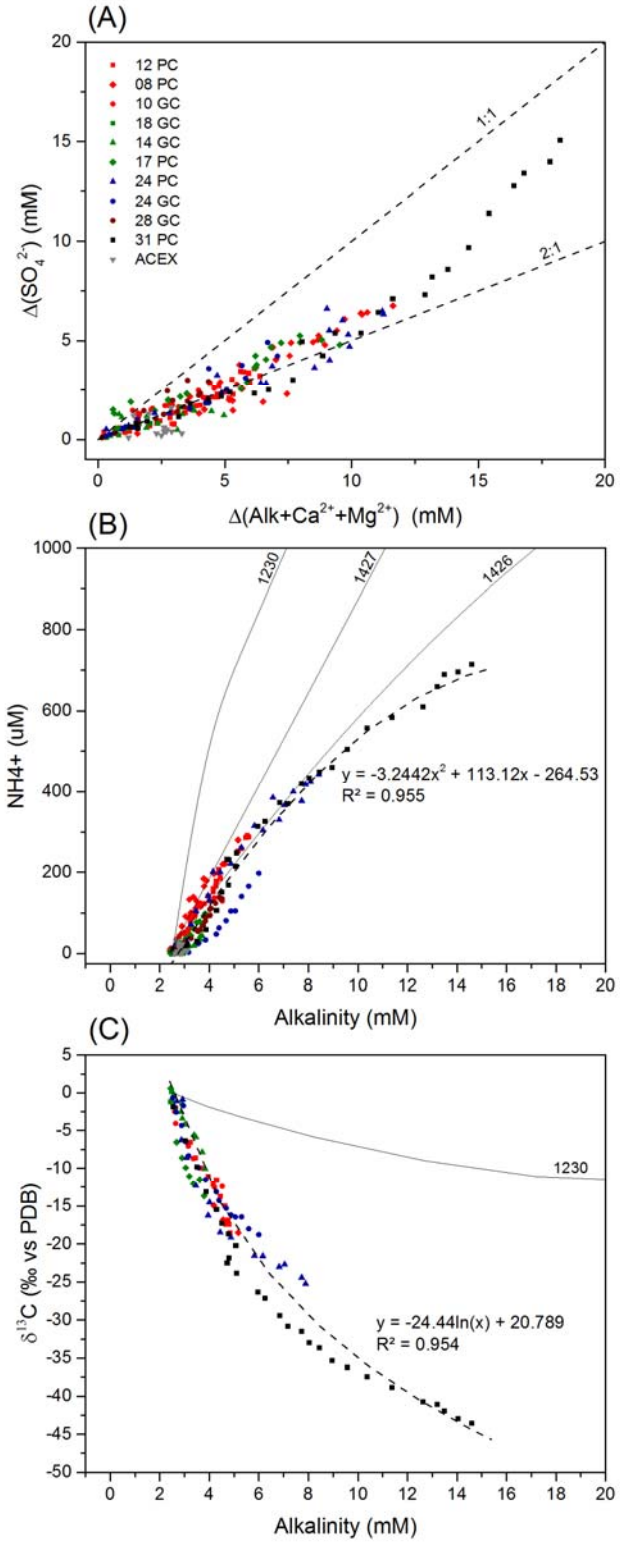

1410

1411 **Figure 10.**

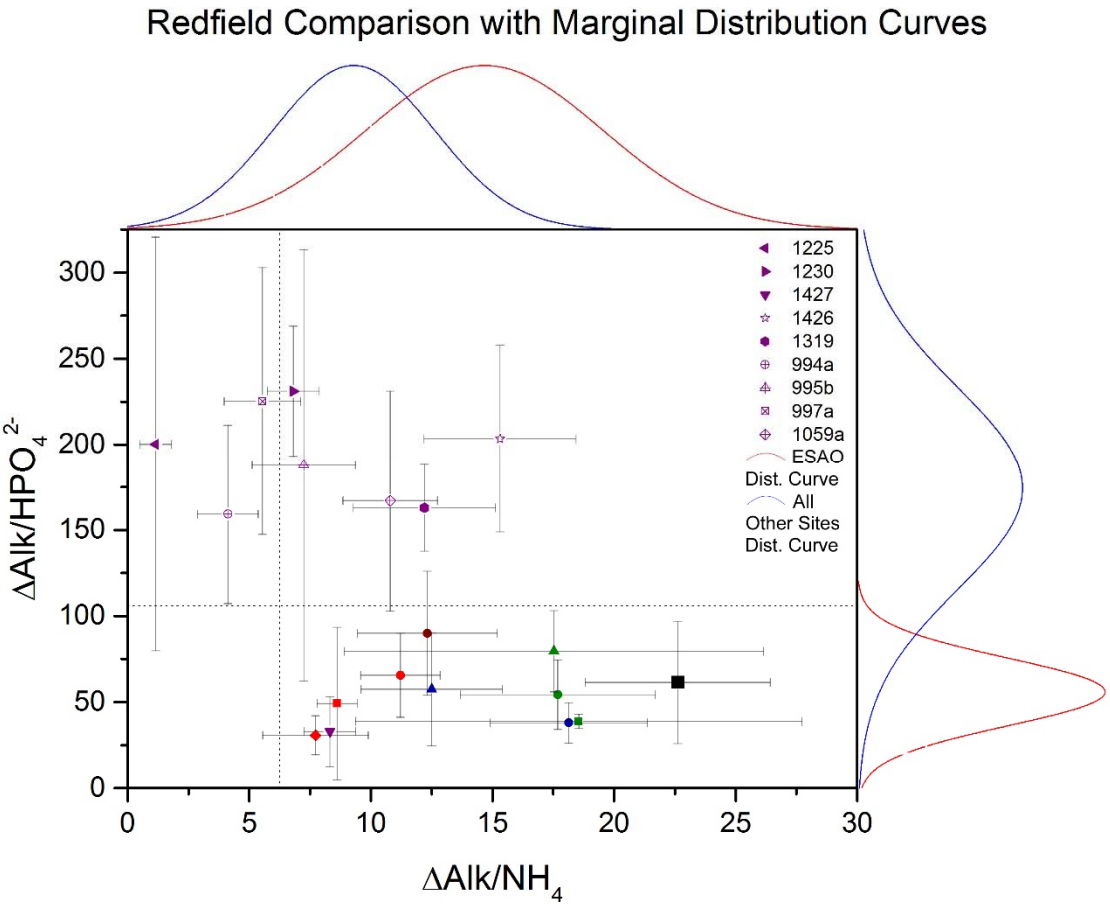

1412

Figure 11.

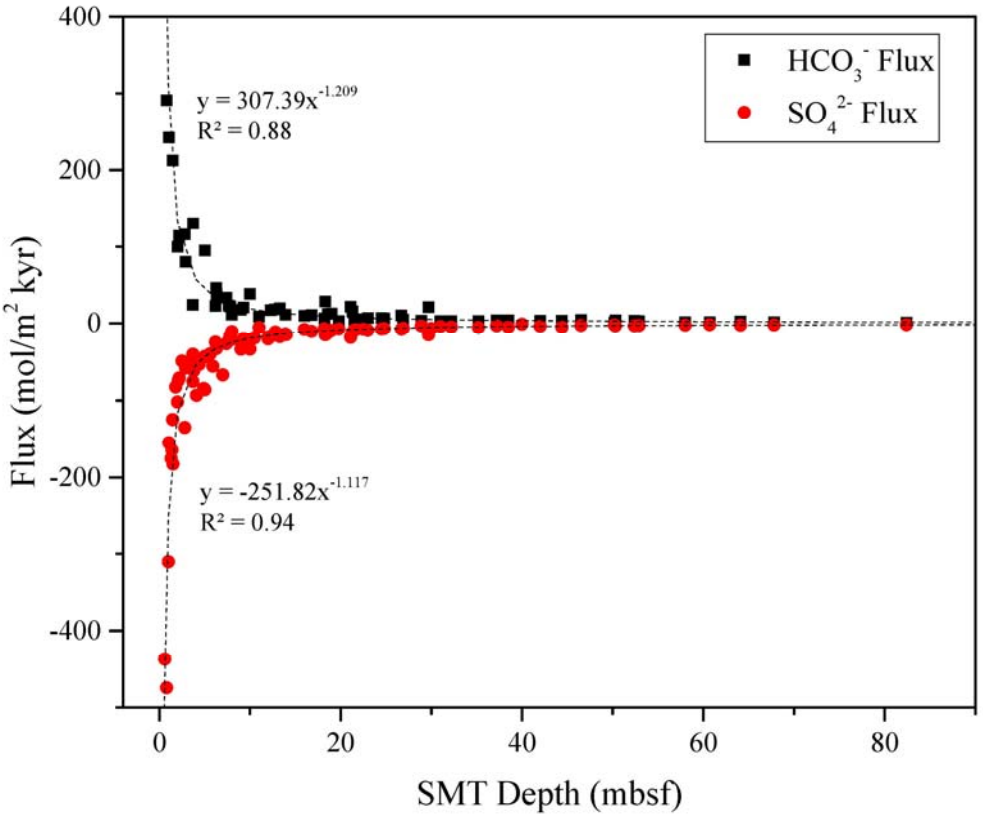
400
200
0
-200
-400
0
20
40
60
80
Flux (mol/m^2 kyr)
SMT Depth (mbsf)
HCO_3^- Flux
SO_4^{2-} Flux
y = 307.39x$^{-1.209}$
R² = 0.88
y = -251.82x$^{-1.117}$
R² = 0.94

Figure 12.

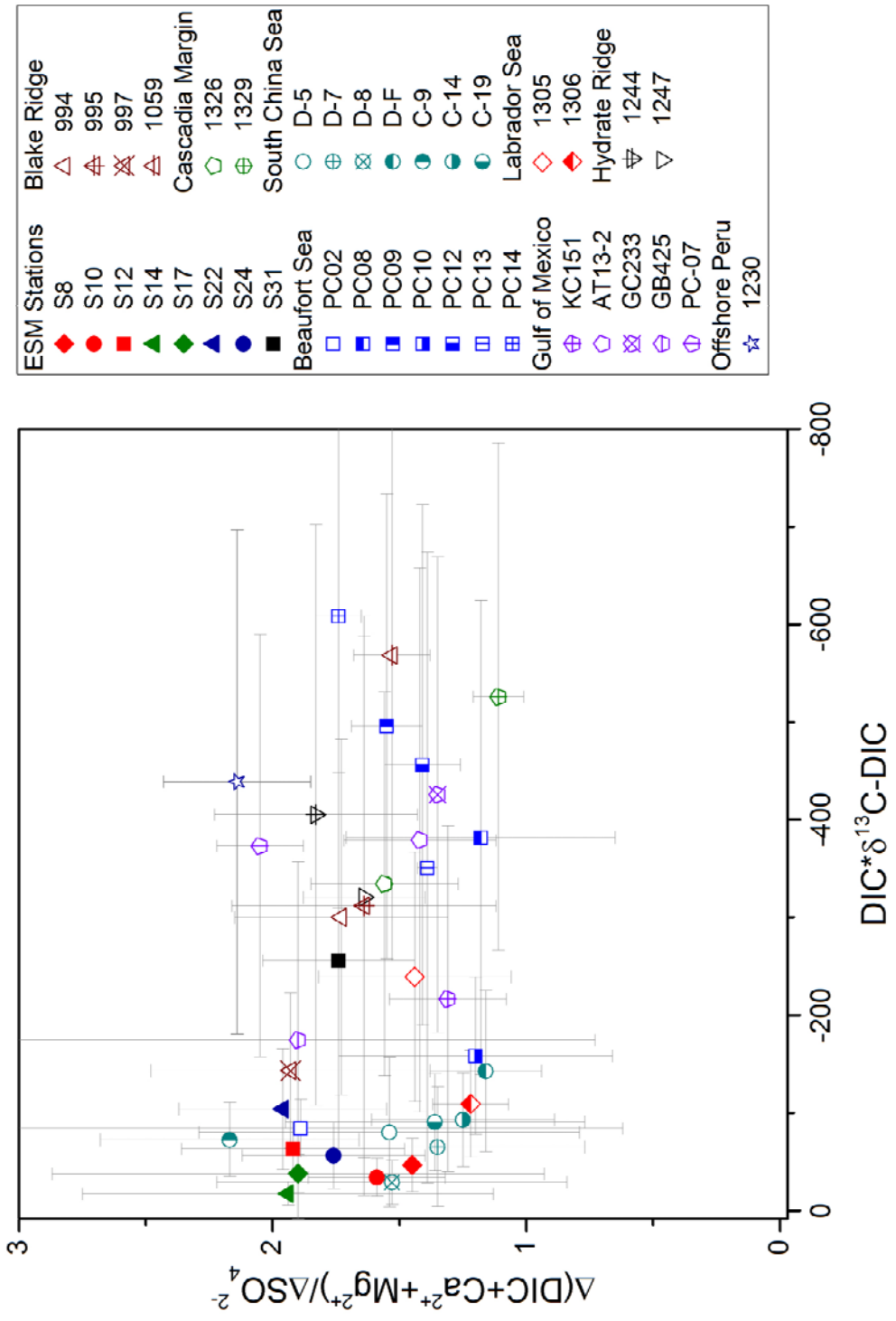
ESM Stations
S8
S10
S12
S14
S17
S22
S24
S31
Blake Ridge
994
995
997
1059
Cascadia Margin
1326
1329
South China Sea
D-5
D-7
D-8
D-F
C-9
C-14
C-19
Labrador Sea
1305
1306
Hydrate Ridge
1244
1247
Beaufort Sea
PC02
PC08
PC09
PC10
PC12
PC13
PC14
Gulf of Mexico
KC151
AT13-2
GC233
GB425
PC-07
Offshore Peru
1230
3
2
1
0
0
-200
-400
-600
-800
Δ(DIC+Ca2++Mg2+)/ΔSO4 2-
DIC*δ13C-DIC

Table 1.

Table 1 QA/QC Results

Analysis	Sample Type	Number	Result
Alkalinity	Spiked	15	PE = 1.53%
Alkalinity	Duplicate	8	PD = 1.30%
δ^{13}C-DIC	Seawater Standard	2	0.23‰ and 0.32‰
δ^{13}C-DIC	Blind Field Duplicate	4	PD = 22.98%
δ^{13}C-DIC	Field Blank	1	No Result
δ^{13}C-DIC	Duplicate	10	PD = 14.70%
Metals	Spiked	51	RSD = 2.55% (Ba), 2.17% (Ca), 1.53% (Fe), 0.77% (Mg), 1.73% (Mn), 1.88% (S), and 1.42% (Sr)
Metals	Blind Field Duplicate	11	PD = 2.56% (Ba), 3.77% (Ca), 5.81% (Fe), 2.68% (Mg), 3.07% (Mn), 0.71% (S), and 3.79% (Sr)
Metals	Field Blank	2	BDL
Phosphate	VKI Standard	2	PE = 1.28% and 2.69%
Ammonia	VKI Standard	2	PE = 2.40% and 6.25%

Notes: PE = Percent Error
PD = Percent Difference
RSD = Relative Standard Deviation
BDL = Below Detection Limit

1439 **Table 2.**

Table 2 - Reported and Calculated Fluxes

Ocean	Location	Water Depth (m)	SMT Depth (mbsf)	SO_4^{2-} Flux (mol/m^2kyr)	Alkalinity Flux (mol/m^2kyr)	$\delta^{13}C$ at SMT (‰)
Arctic	Beaufort Sea - Cape Halkett[a,b]	280	1.06	-154.8	242.6	-21.5
Arctic	Beaufort Sea - Cape Halkett[a,b]	342	1.47	-124.7	212.3	-20.2
Arctic	Beaufort Sea - Cape Halkett[a,b]	1005	3.73	-44.2	130.3	-18.2
Arctic	Beaufort Sea - Cape Halkett[a,b]	1458	6.29	-27.4	46.3	-19.7
Arctic	East Siberian Slope	349	61	-1.8	1.7	--
Arctic	East Siberian Slope	367	25	-6.9	6.3	--
Arctic	East Siberian Slope	384	64	-2.4	2.3	--
Arctic	East Siberian Slope	524	35	-5.6	2.8	--
Arctic	East Siberian Slope	733	58	-2.1	1.5	--
Arctic	East Siberian Slope	977	58	-2.1	1.6	--
Arctic	East Siberian Slope	964	23	-9.2	6.8	--
Arctic	East Siberian Slope	1000	52	-3.3	3.3	--
Arctic	East Siberian Slope	1143	44	-5.1	3.5	--
Arctic	East Siberian Slope	1120	14	-13.9	11.3	--
Atlantic	New Jersey Continental Slope[q,i]	912	28.9	-3.3	3.6‡	--
Atlantic	Blake Ridge[q,p]	1293	50.3	-3.4	3.8‡	--
Atlantic	Blake Ridge[q,p]	1798	26.9	-6.6	4.9‡	--
Atlantic	Blake Ridge[q,x]	2567	42.0	-3.8	3.5‡	--
Atlantic	Blake Ridge[q,x]	2641	24.5	-7.6	6.9‡	--
Atlantic	Blake Ridge[q,x]	2777	21.7	-8.3	5.4‡	--
Atlantic	Blake Ridge[q,x]	2770	22.5	-7.8	4.7‡	--
Atlantic	Blake Ridge[q,x]	2798	21.5	-8.7	4.4‡	--
Atlantic	Blake Ridge[q,p]	2985	9.3	-20.0	20.4‡	--
Atlantic	Blake Ridge[q,p]	3481	12.3	-17.1	17.0‡	--
Atlantic	Blake Ridge[q,p]	4040	16.8	-10.5	10.8‡	--
Atlantic	Gulf of Mexico - Keathley Canyon[w]	1300	9	-33‡	17‡	-49.6
Atlantic	Gulf of Mexico - Atwater Valley[w]	1300	0.1	-2901	--	--
Atlantic	Gulf of Mexico - Atwater Valley[w]	1300	0.1	-2901	--	--
Atlantic	Gulf of Mexico - Atwater Valley[w]	1300	0.6	-437	--	--
Atlantic	Gulf of Mexico - Atwater Valley[w]	1300	7	-67	--	-46.3
Atlantic	Amazon Fan[q,v,y]	3191	37.2	-3.2	4.1‡	-39.8
Atlantic	Amazon Fan[q,v,y]	3474	6.2	-24.6	22.7‡	-47.5
Atlantic	Amazon Fan[q,v,y]	3704	3.7	-40.3	24.3‡	-49.6
Atlantic	Western Africa[q,z]	426	12.8	-12.5	18.2‡	--
Atlantic	Western Africa[q,z]	738	52.9	-3.1	2.9‡	--

Atlantic	Western Africa[q,z]	1280	21.3	-12.0	15.6‡	-19.8
Atlantic	Western Africa[q,z]	1402	18.3	-14.9	28.3‡	--
Atlantic	Western Africa[q,z]	1713	38.5	-5.1	4.1‡	--
Atlantic	Western Africa[q,z]	2179	26.7	-7.8	10.4‡	--
Atlantic	Western Africa[q,z]	2382	21.1	-18.1	21.8‡	--
Atlantic	Western Africa[q,z]	2995	29.7	-14.9	20.9‡	--
Atlantic	Argentine Basin[l]	1228	10.5	-19.1	--	--
Atlantic	Argentine Basin[l]	1492	12	-20.2	--	--
Atlantic	Argentine Basin[l]	1568	4.9	-84.6	--	--
Atlantic	Argentine Basin[l]	1789	5.9	-55.6	--	--
Atlantic	Argentine Basin[l]	3247	10	-21.8	--	--
Atlantic	Argentine Basin[l]	3167	14	-14.7	--	--
Atlantic	Argentine Basin[l]	3542	3.7	-75.4	--	--
Atlantic	Argentine Basin[l]	3551	5.6	-39.9	--	--
Atlantic	Argentine Basin[l]	3551	4.1	-93.3	--	--
Atlantic	Argentine Basin[l]	3623	5	-43.1	--	--
Atlantic	Argentine Basin[l]	4280	5.1	-43.5	--	--
Atlantic	Argentine Basin[l]	4799	12	-17.9	--	--
Indian	Oman[q,1]	591	50.2	-2.2	1.1‡	--
Indian	Oman[q,1]	804	46.5	-2.8	4.4‡	--
Indian	Oman[q,1]	1423	82.4	-1.8	0.8‡	--
Pacific	Bering Sea[p,2]	1008	6.3	-32.8	37.8	-25.1
Pacific	Cascadia[q,u,2]	959	9.0	-23.6	--	-23.8
Pacific	Cascadia[q,u,2]	1322	7.9	-21.3	--	-30.8
Pacific	Cascadia[q,u,2]	1828	2.5	-49.0	--	-33.9
Pacific	Cascadia - Hydrate Ridge[o]	834	8	-10.9	11.3	-19.6
Pacific	Cascadia - Hydrate Ridge[o]	850	7.65	-22.3	23.2	-30.2
Pacific	Cascadia - Hydrate Ridge[o]	871	7.4	-26.6	33.4	-24.9
Pacific	Cascadia - Hydrate Ridge[g]	896	7.8	-16	22	-22.5
Pacific	Umitaka Spur[h]	900	2.2	-71	114	--
Pacific	Umitaka Spur[h]	947	2.9	-58	80	--
Pacific	Umitaka Spur[h]	1034	2.0	-102	100	--
Pacific	Japan Sea[s,4]	901	10	-33.6	38.4‡	--
Pacific	California Margin[q,5]	955	13.3	-17.3	19.6‡	--
Pacific	California Margin[q,5]	1564	19.0	-9.3	12.8‡	--
Pacific	California Margin[q,5]	1926	31.0	-4.3	3.1‡	--
Pacific	Nankai Trough[q,6]	1741	32.2	-4.9	3‡	--
Pacific	Nankai Trough[s,6]	2997	11.0	-5.6	8.7‡	--
Pacific	Nankai Trough[q,6]	3020	18.2	-7.0	6.4‡	--

Pacific	Santa Barbara[k]	587	1.3	-175.2	--	--
Pacific	Soledad[k]	542	1	-310.3	--	--
Pacific	Pescadero[k]	408	1.4	-164.3	--	--
Pacific	Magdalena[k]	600	1.5	-182.5	--	--
Pacific	Alfonso[k]	713	0.8	-474.5	--	--
Pacific	Costa Rica Margin[q,7]	3306	16.0	-8.1	9.6‡	--
Pacific	Costa Rica Margin[q,7]	4177	19.8	-7.5	3.1‡	--
Pacific	Costa Rica Margin[q,7]	4311	18.6	-12.3	12.4‡	--
Pacific	Peru Margin[s,8]	161	30	-6.9	--	--
Pacific	Peru Margin[t,9]	427	40	-1.2	--	-25.4
Pacific	Peru Margin[t,9]	5086	9	-25.0	--	-13.2
Pacific	Chilean Coast[c]	586	5.55	-22.9	--	--
Pacific	Chilean Coast[c]	723	0.33	-362.0	--	--
Pacific	Chilean Coast[c]	980	2.92	-45.3	--	--
Pacific	Chilean Coast[c]	768	10.11	-13.3	--	--
Pacific	New Zealand - Porangahau Ridge[f]	1900-2150	12.8	-11.4	--	-31.4
Pacific	New Zealand - Porangahau Ridge[f]	1900-2150	4.4	-53.3	--	-31.6
Pacific	New Zealand - Porangahau Ridge[f]	1900-2150	3.6	-50.5	--	-31.4
Pacific	New Zealand - Porangahau Ridge[f]	1900-2150	2.1	-74.2	--	-33.4
Pacific	New Zealand - Porangahau Ridge[f]	1900-2150	3.8	-61.5	--	-35.0
Pacific	New Zealand - Porangahau Ridge[f]	1900-2150	1.8	-82.6	--	-48.8
Pacific	New Zealand - Hikurangi[b,d]	350	39.5	5‡	7.3‡	--
Pacific	New Zealand - Hikurangi[b,d]	332	12.9	19.3‡	13.6‡	--
Pacific	New Zealand - Hikurangi[b,d]	98	0.87	192.1‡	160.9‡	--
Pacific	New Zealand - Hikurangi[b,d]	285	3.64	65.2‡	59.6‡	--
Southern Ocean	Antarctic - Cumberland Bay[n]	237	5.03	-86	95	-25.4
Southern Ocean	Antarctic - Cumberland Bay[n]	260	0.80	-539	291	-23.5
Southern Ocean	Antarctic - Cumberland Bay[n]	275	2.80	-135	116	-15.5

1440

1441